Geoscience Frontiers 17 (2026) 102262

Contents lists available at ScienceDirect

Geoscience Frontiers

journal homepage: www.elsevier.com/locate/gsf

Research Paper

The source-to-surface journey of volatile-flooded magmas: The archetypal case of the Campi Flegrei unrest Caldera

Ilenia Arienzo [a,*], Bruna Cariddi [a], Carlo Pelullo [a], Claudia D'Oriano [b], Etienne Deloule [c], Massimo D'Antonio [d], Roberto Moretti [e]

[a] Istituto Nazionale di Geofisica e Vulcanologia, sezione Osservatorio Vesuviano, via Diocleziano 328, 80124 Napoli, Italy
[b] Istituto Nazionale di Geofisica e Vulcanologia, sezione di Pisa, Via Cesare Battisti, 53, 56125 Pisa, Italy
[c] Université de Lorraine, CNRS, CRPG, F-54000 Nancy, France
[d] Dipartimento di Scienze della Terra, dell'Ambiente e delle Risorse, Università degli studi di Napoli Federico II, Complesso Universitario di Monte Sant'Angelo, Via Cinthia 26, 80126 Napoli, Italy
[e] Dipartimento di Ingegneria, Università degli Studi della Campania "Luigi Vanvitelli", Via Roma 29, 81031 Aversa, Caserta, Italy

ARTICLE INFO

Article history:
Received 14 April 2025
Revised 30 November 2025
Accepted 22 January 2026
Available online 25 January 2026

Keywords:
Melt inclusions
Hydrogen isotopes
Volatile elements
H_2O-CO_2-S-melt modelling
δD modelling
Trace elements partition coefficients

ABSTRACT

We attempt to reconstruct the architecture of the magmatic feeding system of the Campi Flegrei volcanic field, currently experiencing an unrest phase threatening several hundred thousand people, to shed light on the processes interplaying during magma evolution and transfer to the surface. To this aim, we provide, for the first time, a complete chemical dataset (major, trace and volatile elements, including hydrogen isotopes) of melt inclusions and their host pyroxenes. Case studies are the Campanian Ignimbrite eruption (~40 ka) and explosive events that occurred in a short time-span (from ~5 ka to ~4 ka), in sectors of the Campi Flegrei caldera identified as having the highest probability of future eruptive activity.

Melt inclusions point to high dissolved volatiles content ($H_2O \approx 0.5–2.9$ wt.%; $CO_2 \approx 120–2600$ ppm; Cl $\approx 4000–10600$ ppm; F $\approx 1400–3400$ ppm; $SO_3 \approx 0.2–0.05$ wt.%) which suggest that magma differentiation and degassing took place at pressures ranging approximately between 645 MPa and 74 MPa. In fact, one of the major outcomes of the paper is the temporary coexistence, at pressures higher than 200 MPa of felsic magma batches with mafic magmas. Modelling of gas release shows that trachytic magmas formed due to crystallization in a system featured by a mean oxidation state with $Fe^{3+}/Fe_{tot} = 0.15$, under variable but high initial volatile contents: total volatiles exceed 5 wt.%, with not less than 2 wt.% CO_2. The high volatile elements content in the deep feeding system is possibly responsible for repeated fluxing events that may prompt the ascent of differentiated magmas to the shallowest reservoirs. Water-loss, due to the combination of repeated crystallization and CO_2 fluxing events in crustal reservoirs, satisfactorily explains the δD variability in melt inclusions, producing multiple paths approaching the δD of the local magmatic water discharged from present-day, low-temperature fumaroles. Our findings suggest that: (1) the studied eruptions were fed by trachytic magma inputs in equilibrium with a gas phase featured by XCO_2 ~0.9 at pressures greater than 250 MPa; (2) XCO_2 decreases nearly continuously while pressure decreases; and (3) the obtained pressures cannot be simply converted into crystallization/storage depths. Conversely, local overpressure associated with gas fluxing must be considered. The overpressure can explain the ascent of differentiated, trachytic magmas that enter the uppermost plumbing system levels with an excess of volatiles, which may drive further magma crystallization and eruption. The final stage of magma ponding and degassing, between ~200 MPa and ~74 MPa, may represent the ultimate engine of the unrest phases at Campi Flegrei that precede volcanic eruptions.

* Corresponding author.
E-mail addresses: ilenia.arienzo@ingv.it (I. Arienzo), bruna.cariddi@ingv.it (B. Cariddi), carlo.pelullo@ingv.it (C. Pelullo), claudia.doriano@ingv.it (C. D'Oriano), etienne.deloule@univ-lorraine.fr (E. Deloule), masdanto@unina.it (M. D'Antonio), roberto.moretti@unicampania.it (R. Moretti).

https://doi.org/10.1016/j.gsf.2026.102262

1. Introduction

Risk mitigation in densely inhabited volcanic areas requires the knowledge and sound interpretation of the behaviour of magma feeding systems and of the possible precursor phenomena of an eruption. Therefore, to contribute to volcanic hazard assessment in areas exposed to volcanic risk, it is important to deepen the knowledge on the geochemical features of the magmas, the architecture of the magma feeding system (number, geometry and depth of reservoirs) and the pre- and *syn*-eruptive magmatic processes that can affect the eruptive dynamics. Chemical analysis of melt and fluid inclusions entrapped in crystals during magma differentiation allow acquiring a large part of information on magma storage and pre-eruptive conditions, as well as on ascent rates (e.g., Esposito et al., 2023; Forte et al., 2023; Zanon et al., 2024). Melt inclusions represent a sort of "snapshot" of a silicate melt and its volatile content at the time of the entrapment. Melt inclusions investigation is a powerful tool for assessing the nature of primitive magmas and their source regions and for defining the physical–chemical conditions of the plumbing systems, their pre-eruptive volatile contents and the degassing processes (e.g., Spilliaert et al., 2006; Blundy and Cashman, 2008; Moore, 2008; Kamenetsky and Kamenetsky, 2010; Mormone et al., 2011; Moretti et al., 2013a,b, 2018a; Di Muro et al., 2014; Cannatelli et al., 2016; Esposito et al., 2018, 2023; Balcone-Boissard et al., 2023). However, the data obtained by the study of melt inclusions must be taken with caution, due to the fact that melt inclusions can be prone to H-diffusion or post entrapment modifications that can make the obtained results unreliable (e.g., Esposito et al., 2018; Barth and Plank, 2021).

Several regions in Italy are characterized by high volcanic risk, particularly the Neapolitan area (e.g., Santacroce et al., 2003; Branca et al., 2023). Within the Neapolitan area, the Campi Flegrei volcanic field (Fig. 1) is in unrest since at least 1950 (e.g., Del Gaudio et al., 2010; De Martino et al., 2021; Chiodini et al., 2022; Tramelli et al., 2022) and the volcanic risk associated to this nested caldera is among the highest on Earth (Orsi et al., 2004). The interpretation of the Campi Flegrei caldera boundaries was debated by many researchers, (e.g., Orsi et al., 1996; De Vivo et al., 2001; Perrotta et al., 2006; Vitale and Isaia, 2014; De Natale et al., 2016; Sbrana et al., 2021), and its structure and boundaries have not been unequivocally defined yet, based on the field data. On the other hand, there is agreement to recognize that the Campi Flegrei volcanic field has been mainly characterized by the emission of compositionally evolved (trachyte and phonolite) products (e.g., D'Antonio et al., 2022, and references therein), since at least ~110 ka (Monaco et al., 2022; Sparice et al., 2024). The few poorly evolved products are shoshonites and latites such as those of Minopoli (11.1 ka; Cannatelli et al., 2007; Arienzo et al., 2016; D'Antonio et al., 2022) and Nisida (~ 4 ka; D'Antonio et al., 1999; Di Renzo et al., 2011) eruptions. K-trachybasalts have been only found as pyroxene- and olivine-hosted melt inclusions in Fondo Riccio, Minopoli and Pomici Principali products (e.g., Cannatelli et al., 2007; Mangiacapra et al., 2008; Arienzo et al., 2016) and in Mg-rich pyroxene-hosted melt inclusions from the Campanian Ignimbrite (Webster et al., 2003).

In recent years, several studies focused in reconstructing the Campi Flegrei plumbing system based on melt inclusions data (e.g., Signorelli et al., 1999; Fulignati et al., 2004; Roach, 2005; Cannatelli et al., 2007; Mangiacapra et al., 2008; Arienzo et al., 2010, 2016; Fourmentraux et al., 2012; Esposito et al., 2018; Voloschina et al., 2018; Moretti et al., 2019; Balcone-Boissard et al., 2024). The published databases mostly include major and volatile elements data. Storage regions between 2 and ~10 km of depth were hypothesized for the Campi Flegrei magmas. Moreover, strong evidences that these magmas carry a huge amount of volatile elements (Cl, F, H_2O), including CO_2, were found (e.g., Roach, 2005; Arienzo et al., 2010, 2016; Esposito et al., 2018). Combined magma crystallization and CO_2 fluxing are among the most important processes determining the highlighted volatile distribution in melt inclusions and the occurrence of CO_2 enrichment in pre-eruptive melts (e.g., Moretti et al., 2013a, b; Caricchi et al., 2018). This volatile specie was suggested to trigger the onset of explosive activity both at closed- and open-conduit volcanoes (e.g., Roach, 2005; Spilliaert et al., 2006; Severs, 2007; Mangiacapra et al., 2008; Arienzo et al., 2010, 2016; Fourmentraux et al., 2012;

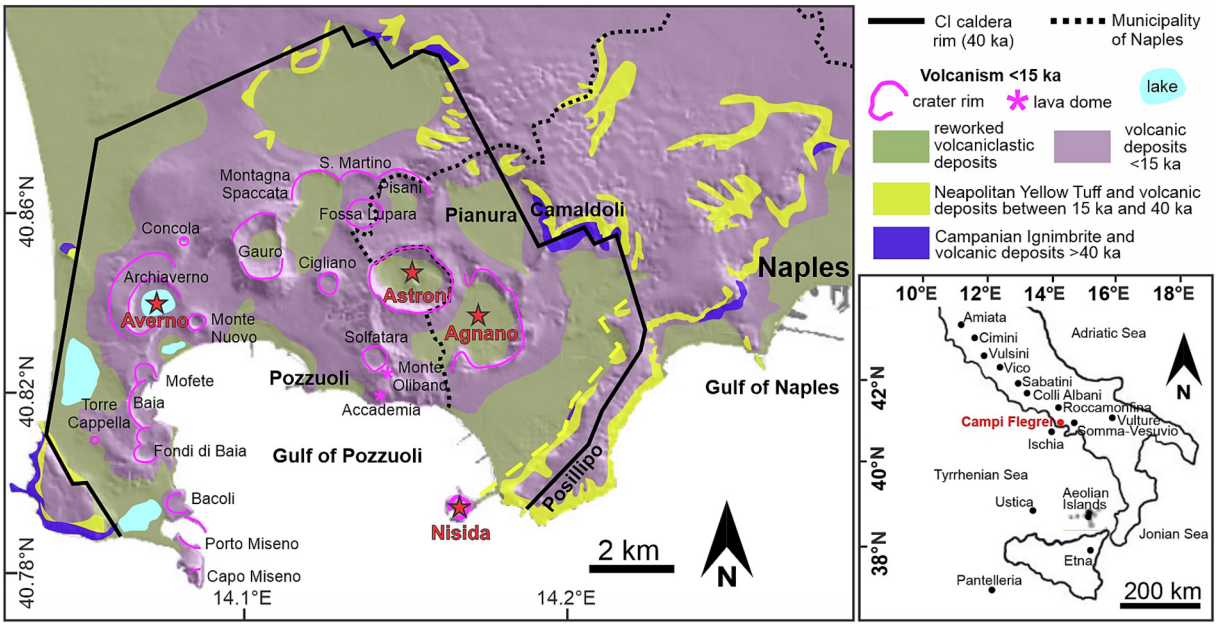

Fig. 1. Simplified geological map of the Campi Flegrei volcanic field. The investigated volcanoes are shown (red stars) together with the Campanian Ignimbrite (CI) caldera boundaries. Solfatara (and Pisciarelli to its NE) geothermal area, featured by major present-day gas emission, and Pozzuoli town (the area of maximum vertical lift), are also shown. Inset: Location of the Campi Flegrei volcanic field (in red) with respect to other Italian volcanoes. Modified after Sparice et al. (2024).

Voloschina et al., 2018; Caricchi et al., 2024). An additional process able to explain the CO_2 enrichment in magmas was presented by Moretti et al. (2019). The authors suggested the possible occurrence of a chromatographic separation between H_2O and CO_2 taking place in extended plumbing systems and leading to early pulses of nearly pure CO_2 and subsequent H_2O enrichment.

In this study, for the first time, we acquired a complete chemical (major oxides, trace and volatile elements) and isotopic (hydrogen) dataset on pyroxene-hosted melt inclusions as well as on their host crystals extracted from Campi Flegrei erupted products. By using the acquired data and by modelling variations in H_2O-CO_2-S and δD in the melt and gas phases, we attempt to shed light on magma degassing, crystallization, ascent, storage and extrusion.

The products of four eruptions occurred between ~5 kyr and ~4 kyr ago (Agnano-Monte Spina, Astroni 6, Averno 2 and Nisida) were selected, three of them occurred in the eastern sector of the Campi Flegrei caldera (Fig. 1). During the last epoch of activity (5.5–3.5 ka; Smith et al., 2011), this sector was characterized by an extensional stress regime, henceforth becoming the most prone to erupt (Orsi et al., 1996, 2004). It was recognized as the area with the highest probability of occurrence of a possible future eruption (Selva et al., 2012; Bevilacqua et al., 2015). Moreover, in order to gather additional information on the ~40 ka Campanian Ignimbrite eruption, we acquired a much larger dataset than the one available in the majority of previous studies (e.g., Signorelli et al., 1999, 2001; Webster et al., 2003; Marianelli et al., 2006; Moretti et al., 2019).

2. Materials and methods

For the purpose of this study, we selected products from: (1) the 4482–4685 cal. years BP (Smith et al., 2011) Agnano-Monte Spina eruption (e.g., de Vita et al., 1999); (2) the Astroni 6 Unit (e.g., Isaia et al., 2004) produced by one of the seven eruptions occurred in the time span between 4345 and 4192 cal. years BP (Smith et al., 2011) in the Astroni area; (3) the ~4.3 ka BP Averno 2 eruption (Pistolesi et al., 2016); (4) the Ar-Ar dated at 3.98 ± 0.53 ka Nisida eruption (Di Renzo et al., 2011), and (5) the 39.85 ± 0.14 ka (Giaccio et al., 2017) Campanian Ignimbrite eruption (Fig. 1). The latter represents the most voluminous and explosive volcanic eruption of the Campi Flegrei, and the most powerful occurred in the Mediterranean area in the last 100 kyr (Orsi, 2022, and references therein). The Agnano-Monte Spina and Astroni 6 eruptions were selected as reference events in case of renewed volcanic activity in the Campi Flegrei caldera, for the largest- and the medium-size explosive events, respectively (Orsi et al., 2009; Bevilacqua et al., 2015). Finally, Nisida and Averno 2 eruptions are both small-size, recent volcanic events at Campi Flegrei caldera showing clear evidence of mixing between compositionally different magmas (Di Vito et al., 2011; Arienzo et al., 2016; D'Antonio et al., 2022).

Pyroxene crystals were hand-picked from pumiceous fragments of: (i) the major fallout layers (A, B and D) of the Agnano-Monte Spina eruption (de Vita et al., 1999), representing the entire chemical variability of the erupted sequence; (ii) layers C and F of the Astroni 6 deposit (Tonarini et al., 2009), displaying the widest chemical and isotopic variability; (iii) Nisida latite (Arienzo et al., 2016); (iv) Averno 2, Member C (Di Vito et al., 2011), the richest in pyroxene grains; and (v) Campanian Ignimbrite products (Moretti et al., 2019).

Specifically, we performed a combined Electron Microprobe (EMP), Laser Ablation-Inductively Coupled Plasma-Mass Spectrometry (LA-ICP-MS) and Secondary Ion Mass Spectrometry (SIMS) study on pyroxene-hosted melt inclusions in order to determine volatile, major and trace element contents and hydrogen isotopes (δD). We considered glassy inclusions free of visible daughter crystals and analysed the chemical composition of the host-pyroxene (Supplementary Material 2, Supplementary Data Table S1) by Scanning Electron Microscope (SEM) and LA-ICP-MS, close to the melt inclusions. Melt inclusions containing bubbles are indicated in Supplementary Material 2, Supplementary Data Table S2.

Due to the fact that post-entrapment crystallization (PEC) can significantly affect the melt inclusions composition (e.g., Danyushevsky et al., 2002) and can modify their original volatile content, the reliability of melt inclusions composition was evaluated before making inferences about magma evolution in the subvolcanic magmatic system. Due to the lack of reliable models to implement the PEC correction for melt inclusions in pyroxene, as also argued by Esposito et al. (2018), the correction was performed by analysing the composition of the host pyroxene and assuming that it was in equilibrium with the melt inclusions. To this purpose, assuming that the appropriate pyroxene-melt K_d $[(XFeO/XMgO)_{cpx}/(XFeO/XMgO)_{melt}]$ for potassic melts (Kamenetsky et al., 1995) is 0.27 ± 0.06 (e.g., Putirka, 2008), we recalculated the melt inclusion composition by using the following equation:

$$Ci_{MI} = (Ci_{cpx} \times \%PEC)/(1-\%PEC)$$

where Ci is major oxides composition and %PEC is the fraction of pyroxene to be added to the corresponding melt inclusion. Details on the number of samples, description of melt inclusions, analytical techniques, operating conditions and utilized standards are provided in Supplementary Material 1. Modelling of the volatile release was carried out by using the non-ideal, composition-dependent model of Papale et al. (2006) and the CHOSETTO software (Moretti et al., 2003; Papale et al., 2022; available at https://github.com/charlesll/chosetto) implemented by accounting for magma crystallization. All the acquired data, as well as data from modelling, are in Supplementary Material 2. Moreover, the acquired data have been made available through Mendeley Data at Arienzo et al. (2026).

3. Results

3.1. Chemistry of the host pyroxene crystals

Pyroxene crystals from the selected eruptive units are diopside with quite homogeneous composition ($Wo_{47-49}En_{35-40}Fs_{13-17}$; Supplementary Material 3, Supplementary Data Fig. S1), and Mg# [molar $Mg^{2+}/(Mg^{2+}+Fe_{tot}) \times 100$] ranging from 69 to 77. Major oxides and trace element contents in pyroxene generally vary in narrow ranges (Al_2O_3 = 2.6–4.8 wt.%, TiO_2 = 0.5–0.9 wt.%, Na_2O = 0.5–0.8 wt.%, CaO = 22.5–23.9 wt.%, Cr < 80 ppm, V < 350 ppm, Ni < 30 ppm; Supplementary Material 2, Supplementary Data Table S1). They do not display significant variations among the selected eruptions, except for some trace elements (e.g., Rb, Ba, K, Sr; Fig. 2), and show no correlation with Mg# (Supplementary Material 3, Supplementary Data Fig. S2). The primitive mantle normalized incompatible trace element patterns show variable Ba, K, Sr, Pb and Ti depletion relative to other trace elements (Fig. 2a). The chondrite-normalized REE (Rare Earth Elements) patterns (Fig. 2b) show slight light REE (LREE) enrichment relative to the heavy REE (HREE; La_N/Yb_N = 2.6–3.9; N stands for normalized to the chondrite) and variable negative Eu anomaly [$Eu/Eu^* = Eu_N/(Sm_N \times Gd_N)^{0.5}$ = 0.35–0.96], which is generally more marked in pyroxene with lower Mg# (Supplementary Material 3, Supplementary Data Fig. S2), indicating that the most evolved magmas had also suffered significant feldspar crystallization.

In terms of trace elements, pyroxene crystals from Agnano-Monte Spina, Astroni 6 and Campanian Ignimbrite pumices show chemical variability. Pyroxene crystals from layers A and B of the Agnano-Monte Spina eruption have higher content in Ba, High

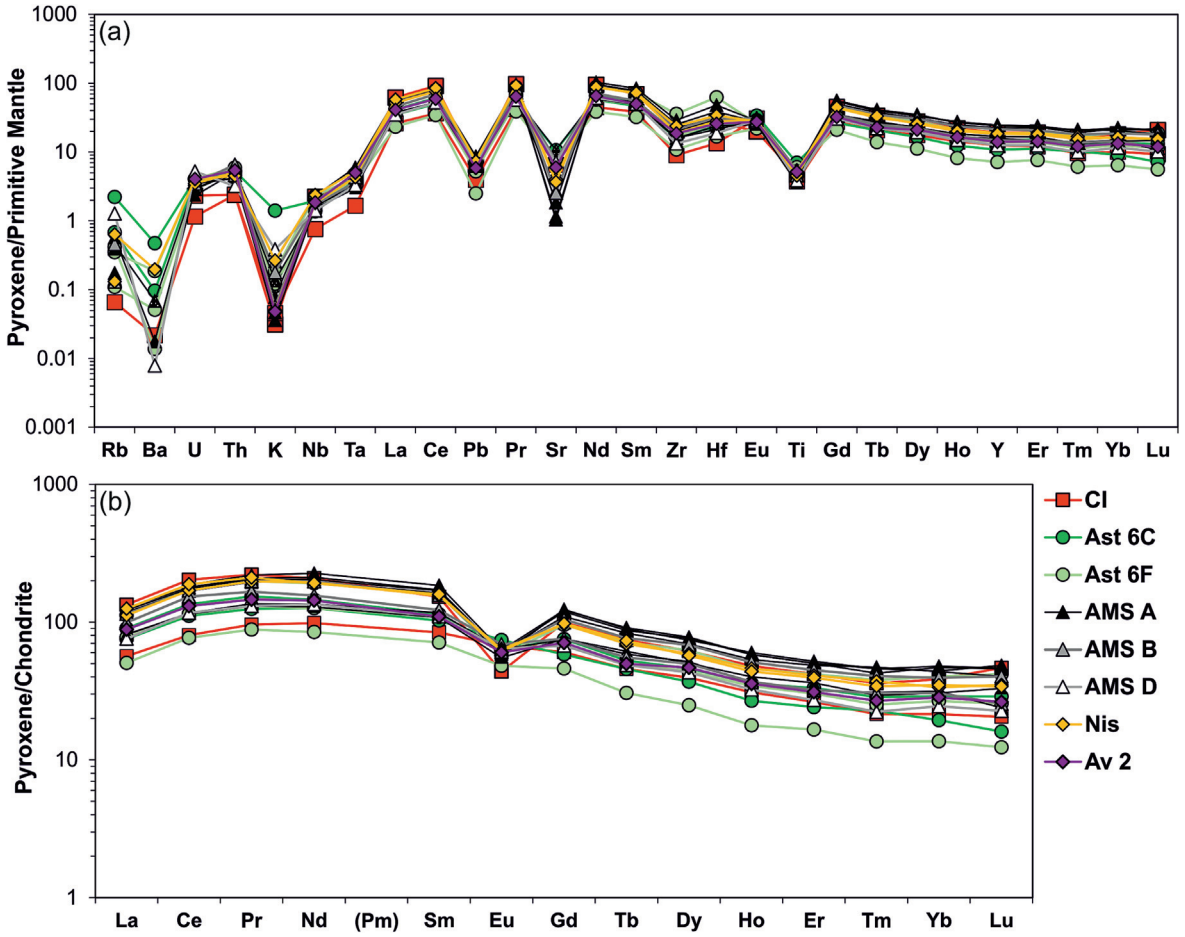

Fig. 2. (a) Primitive mantle normalized incompatible trace element patterns and (b) Chondrite normalized REE patterns of the analysed pyroxene from the studied Campi Flegrei eruptions. Normalization values are from Lyubetskaya and Korenaga (2007) and Anders and Grevesse (1989), respectively. Abbreviations: Cl, Campanian Ignimbrite; Ast 6, Astroni 6; AMS, Agnano-Monte Spina; Nis, Nisida; Av 2, Averno 2.

Field Strength Elements (HFSE) and REE and lower content in Rb, K and Sr relative to pyroxene from layer D. Pyroxene grains from Astroni 6 display variable enrichment in Rb, Ba, K, Sr and REE, with one pyroxene from Astroni 6C layer having the lowest REE content among all the analysed pyroxene crystals. The few pyroxene crystals from Nisida and Averno 2 erupted products are in the compositional range of those from Astroni 6. One pyroxene from Campanian Ignimbrite has the lowest contents of trace elements and displays strong depletion in Sr and Eu (Fig. 2; Supplementary Material 2, Supplementary Data Table S1). The REE patterns of the analysed pyroxene fall within the compositional fields reported in literature for crystals from the same eruptions (Supplementary Material 3, Supplementary Data Fig. S3). Campanian Ignimbrite pyroxene have Mg# from 64 to 93, Astroni from 65 to 92, Agnano-Monte Spina from 45 to 92 and Nisida from 67 to 90 (Forni et al., 2016, 2018; Pelullo et al., 2022b). However, the majority of the Campi Flegrei clinopyroxene have Mg# in the range of 67–78 (e.g., Pelullo et al., 2022a) similar to those of the crystals analysed in this work.

3.2. Chemistry of melt inclusions

The major oxides and trace elements composition of the analysed melt inclusions is reported in Supplementary Material 2, Supplementary Data Table S2. According to the Total Alkali vs. Silica (T. A.S.) classification diagram, the Agnano-Monte Spina melt inclusions are trachytes, the Averno 2 and Campanian Ignimbrite melt inclusions are phonolites, whilst melt inclusions from Nisida and Astroni 6 plot close to the boundary line between the trachyte and phonolite fields (Supplementary Material 3, Supplementary Data Fig. S4). SiO_2 content ranges from 58.6 wt.% to 62.0 wt.%, Al_2O_3 from 17.2 wt.% to 20.1 wt.%, Fe_2O_{3tot} from 3.0 wt.% to 4.7 wt.% and MgO from 0.15 wt.% to 0.84 wt.%. Moreover, CaO varies from 1.1 wt.% to 2.8 wt.%, Na_2O from 3.8 wt.% to 5.4 wt.% and K_2O from 7.0 wt.% to 12.0 wt.%, with the lowest MgO, Fe_2O_{3tot} and CaO, and the highest K_2O contents shown by the Campanian Ignimbrite phonolitic melt inclusion (Fig. 3).

The analysed inclusions overlap the trends depicted by melt inclusions and whole rocks from literature, for the corresponding eruptions (Fig. 3), and more generally are similar to the majority of volcanic products erupted at Campi Flegrei caldera since at least 60 ka ago (e.g., Arienzo et al., 2016). Taking into account literature data, the few relatively poorly evolved (latite and trachybasalt) melt inclusions compositions, in trachytic rocks, are found in Campanian Ignimbrite and Agnano-Monte Spina samples (Webster et al., 2003; Arienzo et al., 2010; Cariddi et al., 2026; Fig. 3, Supplementary Material 3, Supplementary Data Fig. S4).

In general, at decreasing MgO content, Fe_2O_{3tot}, CaO and V contents decrease, whilst SiO_2, Na_2O and Zr contents increase in both the analysed and literature melt inclusions and associated whole rocks (Fig. 3). The correlation between MgO and V or Zr is not observed in few (six in total) melt inclusions from Campanian Ignimbrite, Nisida and Astroni 6 samples (Fig. 3e, f). However, when their trace elements are plotted (e.g., Zr vs. Ce; Fig. 4) these inclu-

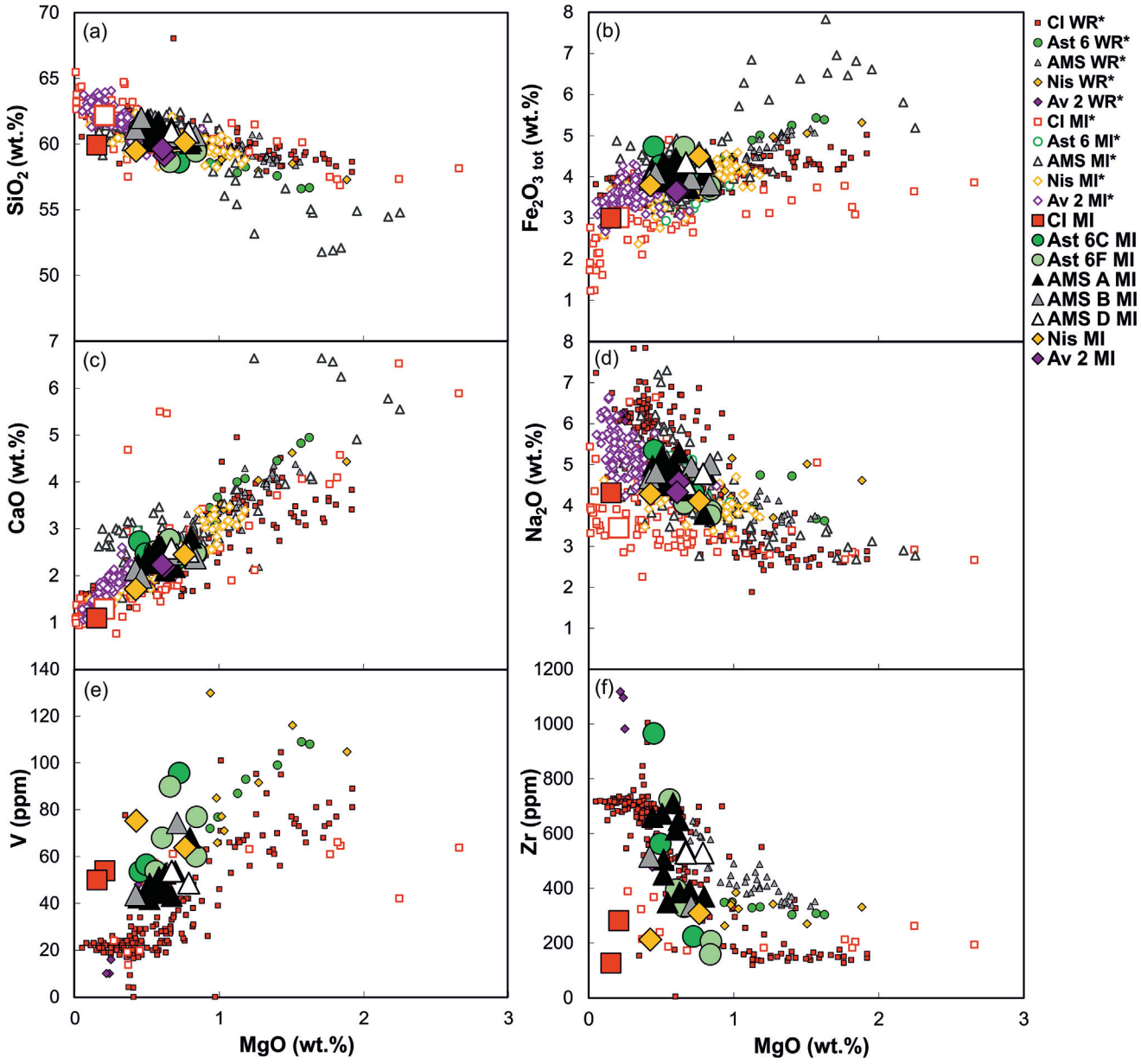

Fig. 3. Diagrams of MgO (wt.%) vs. (a) SiO_2 (wt.%), (b) $Fe_2O_{3\ tot}$ (wt.%), (c) CaO (wt.%), (d) Na_2O (wt.%), (e) V (ppm), (f) Zr (ppm) for the analysed melt inclusions (MI), compared with whole rocks (WR*) and MI* from literature: Cl WR* (Civetta et al., 1997; Signorelli et al., 1999, Marianelli et al., 2006; Fowler et al., 2007; Fedele et al., 2008; Forni et al., 2016, 2018), Ast 6 WR* (Tonarini et al., 2009), AMS WR* (de Vita et al., 1999; Forni et al., 2018), Nis WR* (Melluso et al., 2012; Arienzo et al., 2016; Forni et al., 2018), Av 2 WR* (Fourmentraux et al., 2012), Cl MI* (Signorelli et al., 1999; Fulignati et al., 2004; Marianelli et al., 2006; Severs, 2007; Moretti et al., 2019; Cariddi et al., 2026), Ast 6 MI* (Arienzo et al., 2016), AMS MI* (Roach, 2005; Arienzo et al., 2010; Esposito et al., 2018; Cariddi et al., 2026), Nis MI* (Arienzo et al., 2016; Cariddi et al., 2026), Av 2 MI* (Fourmentraux et al., 2012). Cl MI* data (big size symbol) are major oxide elements published in Moretti et al. (2019), integrated with trace elements from this study. Abbreviations as in Fig. 2.

sions follow the trends defined by whole rocks too. As expected, incompatible trace elements such as Zr, Nb, Rb, Ce increase during magma evolution through fractional crystallization, that is at decreasing MgO content (the latter taken as index of differentiation), as shown in Figs. 3 and 4 (Zr vs. Nb, Zr vs. Rb and Zr vs. Ce diagrams). Sr (not shown) and Ba contents decrease during magma differentiation due to feldspar fractionation (Fig. 4d).

All the analysed melt inclusions, although with evolved composition, have the typical pattern of subduction-related igneous rocks in the incompatible trace elements diagram normalized to the primitive mantle, showing features such as a positive peak in Pb and a depletion in Nb, Ta, Ti (Fig. 5a). Melt inclusions from layers A and B of Agnano-Monte Spina and from layer C of Astroni 6 have the most marked Ba and Sr depletion. Moreover, melt inclusions from Astroni products show the largest chemical variations. A single melt inclusion in Astroni 6 layer C is the most enriched in trace elements and REE among all the analysed inclusions, whilst one melt inclusion from the Campanian Ignimbrite pyroxene is the least enriched (Fig. 5). In the chondrite normalized REE diagram (Fig. 5b), all melt inclusions are enriched in LREE with respect to the HREE (La_N/Yb_N = 13–23) and have variable Eu anomaly (Eu/Eu* = 0.3–1). In the diagram of trace elements normalized to primitive mantle, melt inclusions overlap the patterns of the corresponding whole rock, generally showing a larger variability, and a lower enrichment, in trace elements (Supplementary Material 3, Supplementary Data Fig. S5).

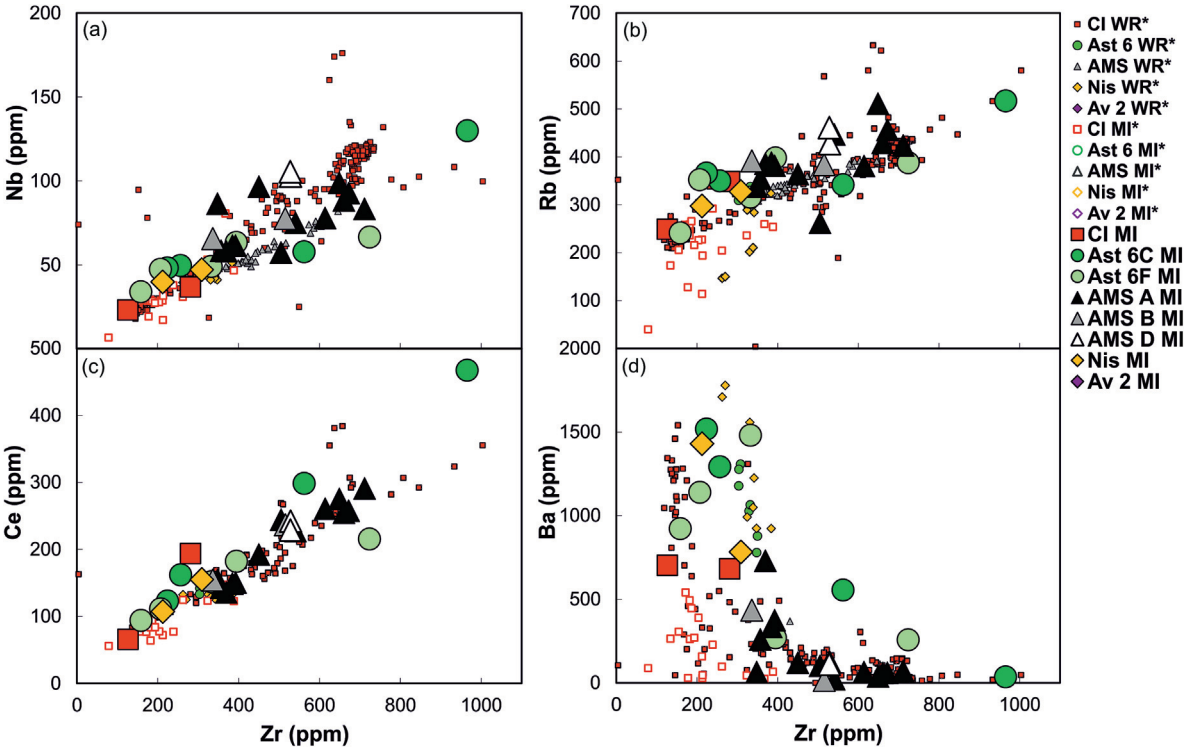

Fig. 4. Diagrams of Zr (ppm) vs. (a) Nb (ppm), (b) Rb (ppm), (c) Ce (ppm), (d) Ba (ppm). Data for the analysed melt inclusions (MIs), are compared with data on whole rocks (WR*) and MI* from literature. References as in Fig. 3.

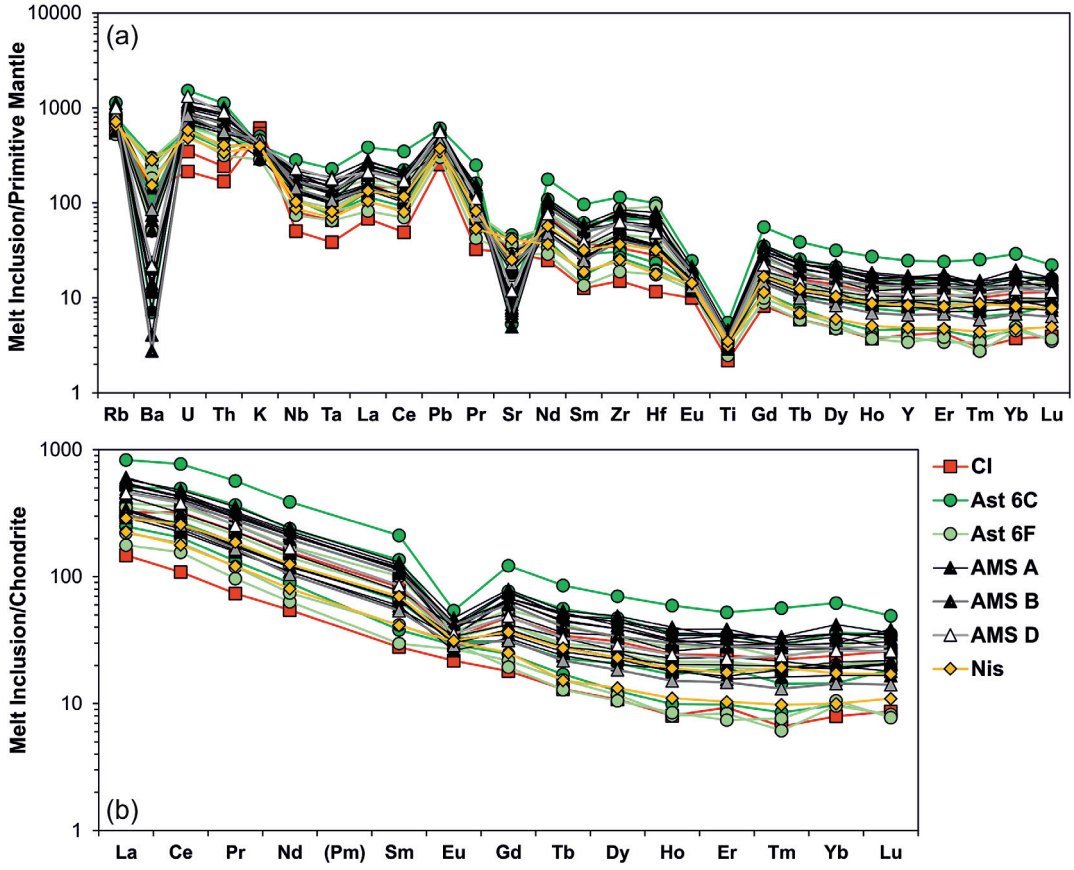

Fig. 5. (a) Primitive mantle normalized incompatible trace element patterns (Lyubetskaya and Korenaga, 2007) and (b) Chondrite normalized REE patterns (Anders and Grevesse, 1989) of the analysed melt inclusions. Abbreviations as in Fig. 2.

3.3. Volatile elements contents in melt inclusions

The volatile elements content (H_2O, CO_2, Cl, F) determined on 43 melt inclusions is reported in Supplementary Material 2, Supplementary Data Table S2. H_2O ranges from 0.51 wt.% to 2.92 wt.% with the highest value detected in one melt inclusion of Astroni 6 layer C and the lowest in one of the Campanian Ignimbrite. CO_2 ranges from 121 ppm to 2666 ppm (0.01–0.27 wt.%). The whole range of variation is found in Agnano-Monte Spina A melt inclusions. SO_3 varies from 0.05 wt.% to 0.20 wt.% (S = 200–801 ppm), with the highest and lowest values in melt inclusions of Nisida and Agnano-Monte Spina, respectively. Cl and F vary from 4061 ppm to 10629 ppm and from 1456 ppm to 3458 ppm, respectively, with the highest values in Agnano-Monte Spina and the lowest values in Campanian Ignimbrite melt inclusions (Fig. 6).

At increasing differentiation index (e.g., at increasing Cl and Zr contents), F slightly increases (Fig. 6a, b), H_2O increases, with two inclusions out of trend, one with lowest (0.5 wt.%) and one with highest (2.9 wt.%) H_2O contents (Fig. 6c, d). No clear correlation is observed between CO_2 and Cl or Zr, particularly when taking into account the few CO_2-richest melt inclusions of Agnano-Monte Spina products (Fig. 6e, f). By excluding them, an inverse correlation is observed. SO_3 decreases at increasing Cl, except for Campanian Ignimbrite melt inclusions from literature showing the opposite trend (Fig. 6g), and at increasing Zr contents from ~200 ppm to ~600 ppm (Fig. 6h). Above 600 ppm of Zr, SO_3 slightly increases. Generally, the H_2O, F, Cl and SO_3 contents overlap data from literature on Campi Flegrei melt inclusions (Fig. 6).

Finally, the delta Deuterium (δD), referred to SMOW, measured on a subset of melt inclusions (Supplementary Material 2, Supplementary Data Table S2) ranges from –41‰ to –137‰, for H_2O contents varying from ~0.5 wt.% to ~2 wt.%. No clear correlation between δD and incompatible elements (Cl and Zr) is observed, except for a slightly negative correlation for some Agnano-Monte Spina melt inclusions (Fig. 6i, j).

3.4. Partition coefficients ($^{cpx/melt}K_d$)

The trace element partition coefficients between pyroxene and trachytic/phonolitic potassic melts from Campi Flegrei products were provided through Instrumental Neutron Activation Analysis (INAA) by Villemant (1988), in situ SIMS analysis of minerals and coexisting glasses by Pappalardo et al. (2008), and LA-ICP-MS analysis on minerals and coexisting glasses by Fedele et al. (2009). Fedele et al. (2009) made an exhaustive discussion of the data presented in Villemant (1988) and Pappalardo et al. (2008) and, therefore, we only focus on the similarities and/or differences between the $^{cpx/melt}K_d$ obtained in this work and the data provided by Fedele et al. (2009).

Using the composition of pyroxene-melt inclusion pairs, trace element partition coefficients have been calculated, and results are shown in Fig. 7 and summarized in Supplementary Material 2, Supplementary Data Table S3. Average partition coefficients are considered for pyroxene hosting more than one melt inclusion. The alkali metals (K, Rb, Cs and Ba) have very low values ($K_d \ll 0.01$). Ti shows negative troughs with respect to the adjacent elements (sorted by increasing atomic number) while Sc, V and Ni show positive peaks (Fig. 7a) for their high compatibility with pyroxene ($K_d \gg 1$). Generally, $^{cpx/melt}K_d$ relative to trachytic and trachyphonolitic melts show similar distribution patterns, with slightly different values only for high atomic mass elements (REEs, Hf, Ta, Th, U and Pb).

The REEs show near-parabolic trends (Fig. 7b) with flat distribution in the Sm–Tm region and with $^{cpx/melt}K_{d(Yb/La)} \simeq 6$ and $\simeq 5$ and $^{cpx/melt}K_{d(Ta/Nb)}$ between $\simeq 4$ and $\simeq 2$, in agreement with the values determined by Fedele et al. (2009) for trachytic and trachyphonolic melts, respectively. Based on Fedele et al. (2009), the most important difference between the compositions of the two melts is the partition coefficient of Eu. The authors found that, in trachytic melts, the $^{cpx/melt}K_d$ for Eu defines an important negative peak that is absent in the trachyphonolitic melts. However, in our melt inclusions, either in trachytic or phonolitic melts, the $^{cpx/melt}K_d$ for Eu displays both peaks and troughs (Fig. 7b) depending on the plagioclase fractionation.

In view of the above considerations, based on the calculated $^{cpx/melt}K_d$, pyroxene 5 and 4 from the Campanian Ignimbrite samples (Supplementary Material 2, Supplementary Data Tables S1, S3) possibly crystallized from a phonolitic and a trachytic magma, respectively. Similarly, crystals from Astroni 6 samples (as well as those from Agnano-Monte Spina) formed in chemically slightly different magmas.

Even if the comparison with literature data suffers from some uncertainties, mainly related to the type of matrix employed as liquid (glass in Fedele et al., 2009, melt inclusion in this work), our calculated partition coefficients are in line with those presented for trachytic and trachyphonolitic melts and calculated on Campi Flegrei juvenile products (Fedele et al., 2009).

4. Discussion

4.1. H-loss, post entrapment crystallization (PEC) and dissolution (PED) in the studied melt inclusions

H-loss from melt inclusions have been discussed by many authors (e.g. Lloyd et al., 2012; Barth and Plank, 2021; Esposito et al., 2023). It has been demonstrated that this process is much more effective in small size melt inclusions, particularly below 40 μm radius. The H-loss is superimposed on the degassing, fluxing and crystallization processes and can be identified, in olivine-hosted melt inclusions by consistent offsets to lower H_2O with respect to K_2O, S, and CO_2 (Lloyd et al., 2012). In Supplementary Material 3, Supplementary Data Fig. S6, the H_2O vs. K_2O diagram shows no evidence of this offset and the melt inclusions follow a main trend of degassing driven crystallization (Barth and Plank, 2021, and references therein). H_2O content displays a linear correlation with respect to S (not shown) and Cl (Fig. 6c), slightly increasing with differentiation, whereas with respect to K_2O (Supplementary Material 3, Supplementary Data Fig. S6), H_2O decreases, varying between 2 wt.% and 1.5 wt.%. One H_2O-rich melt inclusion is also present together with one H_2O-poor melt inclusion from Campanian Ignimbrite. If H-loss occurred, it is limited to few melt inclusions and only slightly modified their initial water content. K_2O and CO_2 (not shown) do not show a clear trend, but for CO_2 contents below 1000 ppm, they appear directly correlated. In addition, Barth and Plank (2021) suggested that if H_2O contents in melt inclusions, or ratios of H_2O contents to incompatible elements correlate with other trace elements, it is possible that the measured H_2O concentrations reflect primary melt compositions. In Supplementary Material 3, Supplementary Data Fig. 7a and b, we show the inverse correlation between H_2O content and incompatible trace elements in the analysed melt inclusions. H_2O/Zr vs. CO_2 (not shown) display the increase in CO_2 content at increasing incompatible trace elements content.

Based on these evidences, we reject the hypothesis that all the analysed Campi Flegrei melt inclusions are affected by significant H-loss. Moreover, the majority of them have more than 100 μm radius, and are located at not less than 200 μm distance from the crystals rim. Only few melt inclusions have less than 100 μm radius. Therefore, even if H-loss cannot be completely ruled out, its impact should be "resized", being the majority of melt inclusions unaffected by post-entrapment processes. On the contrary,

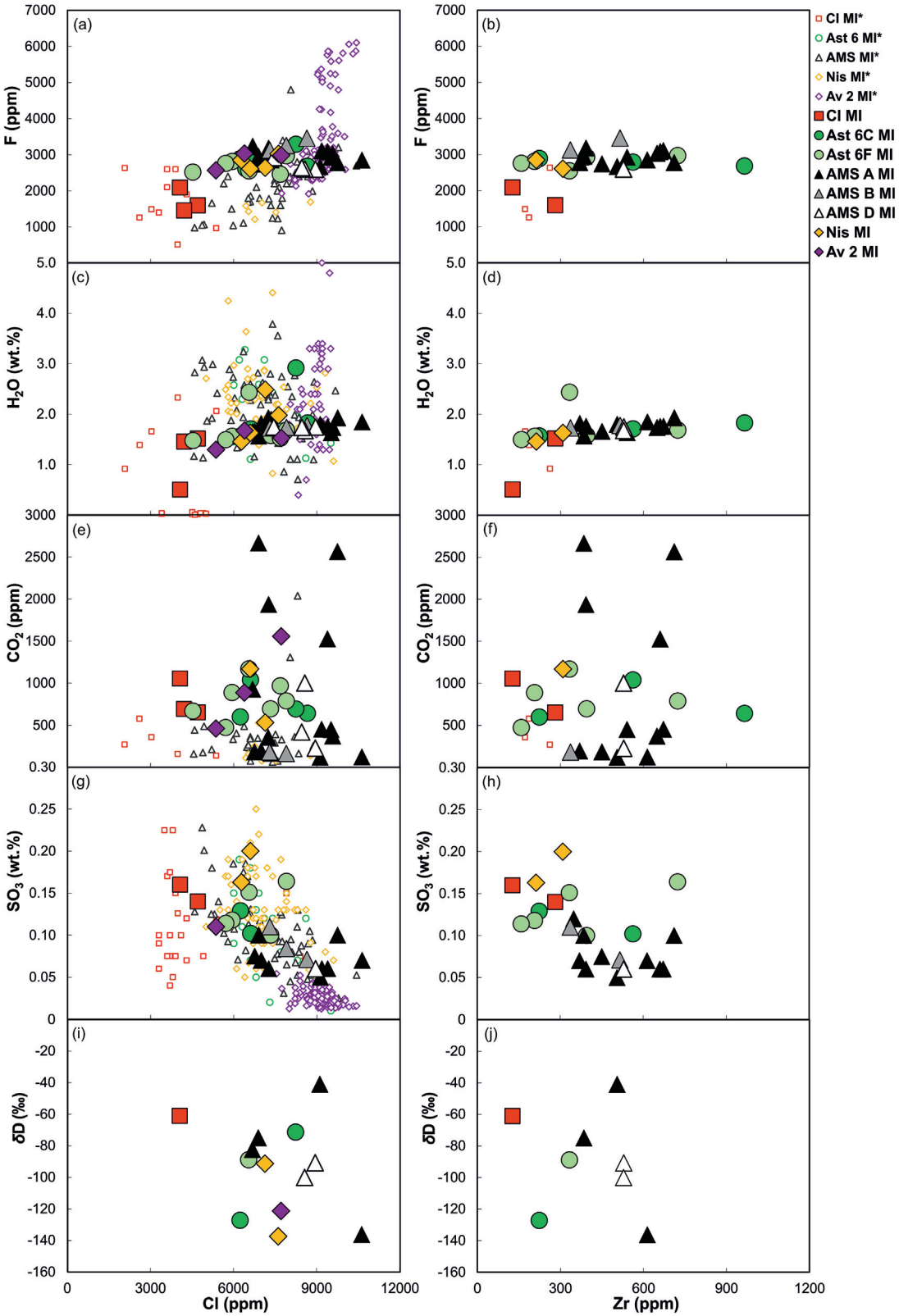

Fig. 6. Diagrams of (a) Cl (ppm) vs. F (ppm), (b) Zr (ppm) vs. F (ppm), (c) Cl (ppm) vs. H_2O (wt.%), (d) Zr (ppm) vs. H_2O (wt.%), (e) Cl (ppm) vs. CO_2 (ppm), (f) Zr (ppm) vs. CO_2 (ppm), (g) Cl (ppm) vs. SO_3 (wt.%), (h) Zr (ppm) vs. SO_3 (wt.%), (i) Cl (ppm) vs. δD (‰), and (j) Zr (ppm) vs. δD (‰), for the analysed melt inclusions (MIs), compared with MI* from literature. Literature data are: Cl MI* (Signorelli et al., 1999, 2001; Fulignati et al., 2004; Marianelli et al., 2006; Severs, 2007; Moretti et al., 2019; Cariddi et al., 2026), Ast 6 MI* (Arienzo et al., 2016), AMS MI* (Roach, 2005; Arienzo et al., 2010; Esposito et al., 2018; Cariddi et al., 2026), Nis MI* (Arienzo et al., 2016; Cariddi et al., 2026), Av 2 MI* (Fourmentraux et al., 2012). H_2O and CO_2 data on Cl MI* (big size symbol), were published in Moretti et al. (2019) whilst their trace elements, Cl, F, S and δD are from this study. Abbreviations as in Fig. 2.

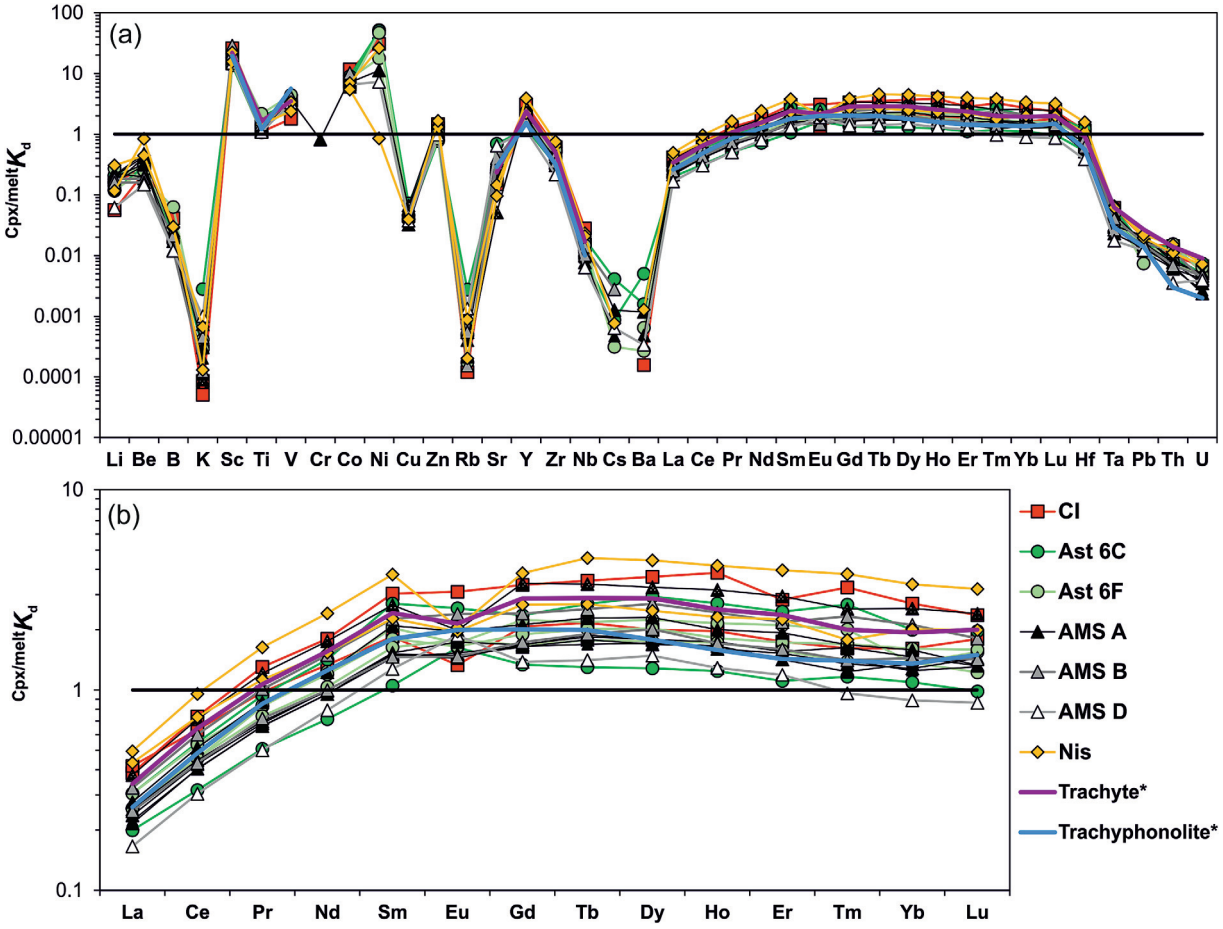

Fig. 7. Calculated $^{cpx/melt}K_d$ values between the analysed melt inclusions and host-pyroxene for (a) trace elements (in increasing order of atomic number) and (b) REE, compared to those calculated by Fedele et al. (2009) in trachytic* and trachyphonolitic* melts from Campi Flegrei. Abbreviations as in Fig. 2.

they more likely reflect primary melt compositions and the CO_2 increase, associated to the H_2O decrease during crystallization, could be due to fluxing.

We also calculated the degree of PEC. It is generally less than 11%. Despite this, the analysed melt inclusions, except for six, generally follow the trends defined by whole rocks (Fig. 3), and can be considered "normal", as defined in Esposito et al. (2018). The PEC-corrected compositions were calculated and reported in Supplementary Material 2, Supplementary Data Table S2, and plotted in Supplementary Material 3, Supplementary Data Fig. S8. When plotted, they are not consistent with the trend of the whole rocks and melt inclusions from literature, particularly for MgO vs. V, Zr, Fe_2O_{3tot} and Na_2O contents, confirming the issues related to the PEC correction for melt inclusions in pyroxene (Esposito et al., 2018) and suggesting a more effective use of the PEC uncorrected compositions. Therefore, based on (i) the relatively low values of the percentage of PEC, (ii) the good correlation between the uncorrected major elements content in melt inclusions and whole rocks literature data, and (iii) the similarity between the calculated partition coefficients (Section 3.4; Fig. 7) with those obtained on Campi Flegrei juvenile products (Fedele et al., 2009), we asses that the PEC effect is negligible and that the trace elements composition, measured in melt inclusions, can well track the evolution of the magma from which pyroxene was crystallizing.

Additional evidences are provided by the $^{cpx/Ml}K_{d\ Fe\text{-}Mg}$ calculated using the uncorrected melt inclusion compositions. Values reported in Supplementary Material 2, Supplementary Data Table S2, are lower compared to the recommended value of ~0.27. However, for the majority of the analysed melt inclusions, no meaningful trends are observed among the $^{cpx/Ml}K_{d\ Fe\text{-}Mg}$ and the volatile elements such as H_2O (Supplementary Material 3, Supplementary Data Fig. S9a). Moreover, covariation diagrams of major and trace elements compatible with pyroxene crystals versus volatile elements content (e.g., V vs. H_2O, Supplementary Material 3, Supplementary Data Fig. S9b) do not display any clear trend or multiple trends that could be associated to a significant role of PEC, such as a marked increasing H_2O content at decreasing V. The alignment we observe can be traced back to fractional crystallization.

The PEC could be also related to the occurrence of vapour bubbles. Indeed, significant amount of CO_2 may enter the vapour bubble during crystallization (Esposito et al., 2011; Steele-Macinnis et al., 2011), particularly in the least evolved melt inclusions, together with H_2O, minor S and Cl (Esposito et al., 2016, and references therein). In some analysed crystals, bubble-free melt inclusions coexist with melt inclusions containing bubbles. Sometimes multiple small bubbles occur, probably due either to the fast depressurization of the system concurrently with fast magma ascent or to entrapment of a melt in which a CO_2-rich gas phase was already partially exsolved (e.g., Capriolo et al., 2020). Despite the presence of bubbles in few melt inclusions, for all the reasons given above, in this study, only the uncorrected chemical analyses were used for the modelling. However, the 6 melt inclusions that in Fig. 3 are out from the main differentiation trend, are the only ones that could be corrected for PEC when their major element content is plotted in binary diagrams for comparison with literatura data.

Therefore, we assume a limited, if any, contribution of the PEC to the chemical composition of the melt inclusions.

The PED process, described in Esposito (2020) must also be excluded. Covariation diagrams of major vs. trace elements compatible in pyroxene (e.g., MgO vs. V, Fig. 3, or V vs. H_2O, Supplementary Material 3, Supplementary Data Fig. S9b), do not show the expected correlation among them. In fact, in case of PED we should observe an increase in the concentration of elements compatible in pyroxene lattice and a decrease in volatile elements. In Supplementary Material 3, Supplementary Data Fig. S9b, the opposite trend is observed. Moreover, we do not see any MgO, CaO and SiO_2 content enrichment in melt inclusions (that will occur in case of PED due to pyroxene dissolution) at similar incompatible (in pyroxene) element contents. Therefore, we exclude any effect related to PED.

4.2. Evolution and degassing of Campi Flegrei magmas based on H_2O-CO_2-S and δD modelling

4.2.1. Modelling of melt saturation pressures and gas composition

The major elements composition of the melt inclusions characterized only for their volatile contents was assumed to be equal to the mean composition of melt inclusions belonging to the same eruption/eruptive unit (Supplementary Material 2, Supplementary Data Table S2). These compositions allow us to derive the saturation pressure for each melt inclusion using the non-ideal, composition-dependent model of Papale et al. (2006). The same model was applied for obtaining the isobars (Supplementary Material 2, Supplementary Data Table S4) at pressures up to 500 MPa, using as starting composition the averaged trachytic composition of all analysed melt inclusions, regardless of the eruption. A constant 1223 K value of temperature was assumed, based on the results reported in Roach (2005) and Pelullo et al. (2022a).

Since the different proportions of FeO and Fe_2O_3 in the melt affect the isobars shape, calculations were carried out by using Fe^{3+}/Fe_{tot} = 0.5 and Fe^{3+}/Fe_{tot} = 0.15 (corresponding to FeO/Fe_2O_3 = 1 and 5, respectively; Supplementary Material 2, Supplementary Data Table S4). The former ratio is in agreement with Vetere et al. (2011) and Moretti et al. (2013a) for poorly differentiated rocks, the latter is in agreement with the ratios determined on evolved Campi Flegrei rocks (Melluso et al., 2012). Due to the evolved composition of the analysed melt inclusions, in Fig. 8a, only curves calculated with Fe^{3+}/Fe_{tot} = 0.15 are plotted. Redox-induced differences are observed between the resulting isobars, when comparing results in Fig. 8a with those in Supplementary Material 3, Supplementary Data Fig. S10, obtained with Fe^{3+}/Fe_{tot} = 0.5. The differences are mostly related to the different proportions of dissolved CO_2 and H_2O, which in turn affect the curvature of the isobars for pressures higher than 250 MPa and water contents between 3 wt.% and 5 wt.%.

Curves with constant H_2O/CO_2 ratios in the gas phase in equilibrium with the melt (Curves 0, 1 and 2 in Fig. 8a) were calculated for the two different Fe^{3+}/Fe_{tot} ratios and at different pressures (Supplementary Material 2, Supplementary Data Table S4). The leftmost Curve 0 corresponds to H_2O and CO_2 contents of 10 mol% and 90 mol%, respectively. Curve 1 corresponds to H_2O and CO_2 contents of 25 mol% and 75 mol%, respectively, whilst Curve 2 corresponds to H_2O and CO_2 contents of 50 mol% and 50 mol%, respectively.

Some analysed melt inclusions (11%) cluster around 50–100 MPa, the remaining record CO_2 contents continuously increasing from 150 MPa up to 400 MPa. Four melt inclusions above the 400 MPa isobar are from Agnano-Monte Spina Unit A, one is from Averno 2 (Fig. 8a). The majority of melt inclusions from Astroni 6, Averno 2 and Agnano-Monte Spina align along, or are very close to,

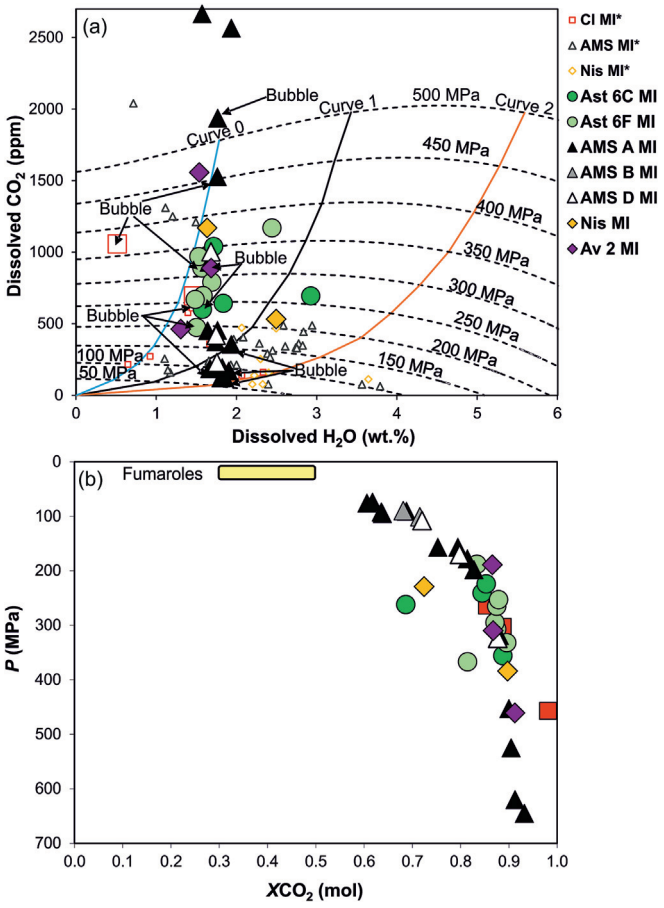

Fig. 8. (a) Dissolved H_2O (wt.%) vs. dissolved CO_2 (ppm) diagram. Isobars were calculated with the model of Papale et al. (2006). A pressure range from 50 to 500 MPa, an average trachytic composition for the melt, temperature of 1223 K and Fe^{3+}/Fe_{tot} = 0.15 were used for calculations. Curves at constant proportion of H_2O and CO_2 in the gas phase were calculated. Curve 0 corresponds to H_2O = 10 mol% and CO_2 = 90 mol%, Curve 1 to H_2O = 25 mol% and CO_2 = 75 mol%, Curve 2 to H_2O = 50 mol% and CO_2 = 50 mol%; (b) XCO_2 (molar fraction) vs. saturation pressures (MPa), obtained with the model of Papale et al. (2006), at temperature of 1223 K for Fe^{3+}/Fe_{tot} = 0.15. The semi-transparent yellow field represents the XCO_2 of the magmatic gas feeding the hydrothermal system at the present-day Campi Flegrei fumaroles (e.g., Caliro et al., 2007). References as in Fig. 6.

Curve 0, displaying a sharp decrease in CO_2 contents at small H_2O content variations. This feature indicates that the magmas of the investigated Campi Flegrei eruptions were in equilibrium with a CO_2-rich gas phase (90 mol%) at high pressures. Furthermore, most of the Agnano-Monte Spina melt inclusions with CO_2 < 500 ppm fall close to the H_2O-rich Curves 1 and 2, and seem to be aligned along isobars between 100 and 150/200 MPa. This feature becomes even more evident when considering literature data acquired on melt inclusions from the same eruption (Arienzo et al., 2010; Cariddi et al., 2026). No difference is observed in the volatile content of the bubble-bearing and the bubble-free melt inclusions (Fig. 8a; Supplementary Material 2, Supplementary Data Table S2). They both contain high and low CO_2 contents and relatively high and low H_2O contents.

Finally, using the major oxides composition of each melt inclusion and the measured H_2O-CO_2 pairs, saturation pressures varying from 74 MPa to 645 MPa were obtained (Supplementary Material 2, Supplementary Data Table S2). Different saturation pressures are obtained (P = 106–564 MPa) when Fe^{3+}/Fe_{tot} = 0.5 is used for calculations. Calculations also return the composition of the gas phase (XCO_2 molar fraction) in equilibrium with the rising magma.

At pressures decreasing from 645 to 74 MPa, the XCO_2 decreases nearly continuously from 0.93 to 0.70–0.60, revealing a trend dominated by decompression and CO_2 degassing (Fig. 8b). Consequently, at shallow depth the gas phase composition tends towards the values inferred for the magmatic gas currently feeding the Solfatara (Fig. 1) hydrothermal system (XCO_2 = 0.32 in Caliro et al. (2007, 2014); XCO_2 = from 0.3 to 0.5 in Moretti et al. (2013b)). The difference between the values recorded by melt inclusions and those currently measured at Campi Flegrei during the monitoring activity is ascribable to the fact that melt inclusions record pre-eruptive values, which refer to a temporally defined entrapment event.

4.2.2. H_2O-CO_2-S-melt and δD modelling

A joint H_2O-CO_2-S-(δD)-melt modelling was used for reproducing the distribution of volatile elements contents and the δD variations in the melt and gas phases, in order to constrain the set of physical–chemical conditions and the processes able to explain their distribution/variability. The acquired data allow modelling simultaneously H_2O-CO_2, H_2O-S, CO_2-S and H_2O-δD covariations and putting more stringent constraints on the values of the initial total (exsolved + dissolved) contents of H_2O, CO_2, S, and iron oxidation state (Fe^{3+}/Fe_{tot}).

To this purpose, we used the CHOSETTO code (Moretti et al., 2003; Moretti and Papale, 2004; Papale et al., 2022) that models volatiles components, reconstructing the degassing patterns in relation with magma decompression, fractional crystallization as well as volatile fluxing (e.g., Aiuppa et al., 2007, 2010, 2022; Edmonds et al., 2010; Pino et al., 2011; Moretti et al., 2013a,b, 2018, 2019; Burton et al., 2023).

For the H_2O-CO_2-S modelling we used the same parameters used in Section 4.2.1 (the mean trachytic composition in Supplementary Material 2, Supplementary Data Table S2, T of 1223 K and two redox conditions: Fe^{3+}/Fe_{tot} = 0.15 and Fe^{3+}/Fe_{tot} = 0.5). Using different, fixed iron ratios is the best approach for evaluating how this parameter controls the S release in its oxidized (SO_2) and reduced (H_2S) forms and for exploring the effects of fO_2 variability.

Degassing runs were conducted under either closed or open-system conditions starting from 600 MPa, considering different initial total (i.e., gas + melt phases) volatile contents. In open-system degassing conditions, at each decompression step, 5 wt.% of the gas phase equilibrated in the previous calculation step was removed from the system. Given the key role played by magma differentiation on volatile release, degassing runs in open-system conditions were also performed by including crystallization. We account for the following pressure-dependent crystallization equation (see Marini et al., 2011; Moretti et al., 2013b, 2018a).

$$XX_{(from0.1-35)} = -0.0582P + 35\ (MPa) \quad (1)$$

where XX is the percentage of crystallization and P is the pressure. The equation assumes a maximum of 35% crystallization while decompressing from 600 to 0.1 MPa. Fig. 9 summarizes the results of modelling for Fe^{3+}/Fe_{tot} = 0.15. Black and red lines refer to closed and open-system degassing conditions, respectively. Blue lines reproduce open-system degassing acting together with magma crystallization. Solid and dashed lines refer to the different, initial, total contents of S. In Supplementary Material 3, Supplementary Data Fig. S11, results of modelling with Fe^{3+}/Fe_{tot} = 0.5, are shown. Data are reported in Supplementary Material 2, Supplementary Data Table S5.

The distribution of the volatiles content in melt inclusions was modelled starting from plausible values of initial total volatile contents (H_2O^T, CO_2^T, S^T) in the gas and melt phases. Based on Mangiacapra et al. (2008), Arienzo et al. (2010) and Moretti et al. (2013b, 2019) and on findings from fluid geochemistry, showing

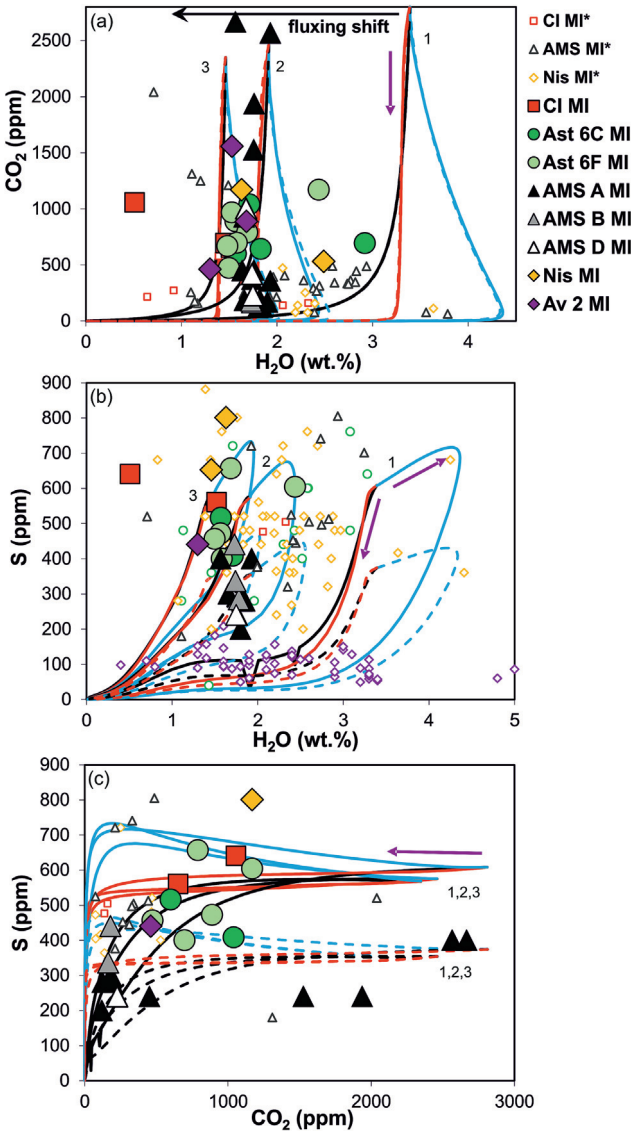

Fig. 9. (a) H_2O (wt.%) vs. CO_2 (ppm), (b) H_2O (wt.%) vs. S (ppm) and (c) CO_2 (ppm) vs. S (ppm) diagrams, showing the melt inclusions data and the modelled degassing paths (two groups of Curves 1, 2, 3: solid and dashed) for a trachytic magma, computed assuming different values of total, initial H_2O, CO_2, S contents. Degassing paths (coloured solid and dashed lines) were calculated by using the CHOSETTO code (Moretti et al., 2003; Papale et al., 2022), assuming T of 1223 K and Fe^{3+}/Fe_{tot} = 0.15. Black and red lines refer to closed and open-system degassing conditions, respectively. Blue lines reproduce open-system degassing acting together with magma crystallization. Solid and dashed lines refer to initial S^T contents of 650 ppm and 400 ppm, respectively. Purple arrows indicate the direction of the degassing trends. References as in Fig. 6.

that the shallow magmatic fluids entering the hydrothermal system are featured by high CO_2 contents and comparable molar proportions of H_2O and CO_2 (Caliro et al., 2007), three groups of curves were generated, having different combinations of H_2O^T and CO_2^T as initial values (Fig. 9). Curve 1 were generated by using H_2O^T = 3.5 wt.% and CO_2^T = 2 wt.%, Curves 2 and 3 by using two sets of equimolar H_2O-CO_2 total volatile contents: H_2O^T = 2 wt.% and CO_2^T = 4.9 wt.%, H_2O^T = 1.5 wt.% and CO_2^T = 3.7 wt.%, respectively (Supplementary Material 2, Supplementary Data Table S5). In terms of initial S^T, a total content of 650 ppm was considered for the trachytic melt inclusions, based on the S contents in melt inclusions with the highest values of dissolved H_2O (Fig. 9b, solid lines; Supplementary Material 2, Supplementary Data Tables S2 and S5).

However, based on the S vs. CO_2 covariation (Fig. 9c), a S^T content of 400 ppm was also used as initial value (dashed lines), at least for reproducing the variability of melt inclusion from Agnano-Monte Spina eruption. This low value could be compatible with a compositionally different initial magma, relatively S-depleted.

In Fig. 9a, which considers CO_2 and H_2O only, either closed or open system degassing regimes (better if including crystallization) can explain the variability shown by most of our data, irrespective of the oxidation state and of the eruption (see Supplementary Material 3, Supplementary Data Fig. S11 for calculations at Fe^{3+}/Fe_{tot} = 0.5). However, the distribution of the data that partially overlap the groups of Curves 2 and 3 further suggests the occurrence of gas fluxing. Following Caricchi et al. (2018), we verify such a possibility by combining major, trace element data and the calculated XH_2O (molar fraction) and XCO_2 (Supplementary Material 2, Supplementary Data Table S2). As expected and shown by other evidences discussed in Section 4.1, at decreasing CaO due to crystallization, XH_2O tends to decrease, whilst XCO_2 increases (Supplementary Material 3, Supplementary Data Fig. S12). When plotted with respect to Zr content we observe a roughly constant XCO_2 (not shown). Fluxing could explain the progressive switch from the relatively H_2O-rich conditions of the melt (H_2O^T = 3.5 wt.% and CO_2^T = 2 wt.%) to the relatively dehydrated and CO_2-enriched ones (e.g., H_2O^T = 1.5 wt.% and CO_2^T = 3.7 wt.%). This latter composition, typical of a gas phase extremely rich in CO_2, represents a vapour-buffered condition, and corresponds to the locus of points having a constant gas composition with XCO_2 = 0.9, in Fig. 8 (or m_{CO_2}/m_{H_2O} = 22 by weight; see also Moretti et al., 2013b). Moretti et al. (2013b) suggested that this condition is achieved in a gas-dominated system, virtually unaffected by CO_2 and H_2O exchanges between melt and gas upon depressurization. This condition could explain the large CO_2 flux measured at the ground level in the Campi Flegrei caldera. It is currently of above 16000 g/(m^2 × day) in the Pisciarelli area (Bollettini di sorveglianza, Osservatorio Vesuviano: https://www.ov.ingv.it/index.php/monitoraggio-e-infrastrutture/bollettini-tutti, accessed 8 April 2025).

Conversely, when taking into account S, the distribution of CO_2, H_2O and S in our melt inclusions is reproduced only assuming the combined effect of open-system degassing, crystallization and variations in the oxidation state. This combination may explain the general trend of S reduction from the least evolved (~3000 ppm; e.g., Mangiacapra et al., 2008; Arienzo et al., 2016) to the most evolved magmas (below 1000 ppm; Fig. 9; e.g., Arienzo et al., 2016), as well as local S enrichments when considering different eruptions. At constant oxidation state (e.g., for Fe^{3+}/Fe_{tot} = 0.15, Fig. 9), local S-enrichment in the melt could be favoured by an open-system degassing, that causes the less soluble CO_2 to be removed (with the consequent relative increase of H_2O and S), either by crystallization, or by a combination of both processes.

Summarizing, most of our data can be explained by considering a trachytic magma that evolves by crystallization (of mostly feldspar and pyroxene) under oxidated conditions (Fe^{3+}/Fe_{tot} = 0.15), and assuming a combination of closed-, open-system degassing and fluxing, starting from a system with H_2O^T = 3.5 wt.%, CO_2^T = 2 wt.% (or close to Curve 1 in Fig. 9) and S^T from 400 ppm to 650 ppm. We cannot rule out completely the possibility that some melt inclusions may have been affected by H-Loss and/or PEC (Esposito et al., 2023, and references therein). In any case, the occurrence of few melt inclusions that may have been affected by these processes, will not invalid the fluxing hypothesis as well as will not affect the general interpretation of the architecture and dynamics of the Campi Flegrei plumbing system, which is based on the whole set of chemical data acquired so far in this and literature papers.

The investigated melt inclusions offered the possibility to retrieve information on the original δD of magmatic fluids at Campi Flegrei and on the processes leading to its variations. Since we are dealing with deep trapped melt inclusion, we exclude the contribution of external fluids, such as the meteoric water, in determining variations in δD, and for the reasons reported in Section 4.1 we exclude effect of H-loss in determining data dispersion. On the contrary, these variations were reproduced by considering that the bulk hydrogen-isotope fractionation between water vapor (H_2O) and melt ($\Delta D_{vapor-melt}$) is a function of the relative amounts of hydroxyl and molecular water in the melt and of the fractionation factor relative to H_2O vapour for each species:

$$\Delta D_{vapor-melt} = \delta D_{vapor} - \delta D_{melt} = Y_{H_2Omelt} \times \Delta D_{vapor-H_2Omelt} + (1-Y_{H_2Omelt}) \times \Delta D_{vapor-OHmelt} \quad (2)$$

where $Y = H_2O_{mol}/(H_2O_{mol} + OH)$; $\Delta D_{vapor\text{-}melt} = \delta D_{vapor} - \delta D_{melt}$, $\Delta D_{vapor\text{-}H_2Omelt} = \delta D_{vapor} - \delta D_{H_2Omelt}$, and $\Delta D_{vapor-OHmelt} = \delta D_{vapor} - \delta D_{OHmelt}$ (Holloway and Blank, 1994). De Hoog et al. (2009) satisfactorily approximated Eq. (2) to the following temperature independent function:

$$\Delta D_{vapor-melt} = 44.53 \times (C_{H_2O}/7.03 + 1)^{-1.2} \quad (3)$$

with C_{H_2O} as the concentration of bulk dissolved water in wt.%.

According to Taylor (1986), due to the fact that $\Delta D_{vapor-melt} \approx 1000 \ln\alpha$, the patterns of isotope fractionation under closed- and open-system (Rayleigh distillation) conditions of water extraction from the melt, are given by:

$$\delta D_{melt} = \delta D_i - (1 - F) \times 1000 \ln\alpha \quad (4)$$

and

$$\delta D_{melt} = \delta D_i - (1000 + \delta D_i) \times (1 - F^{\alpha - 1}) \quad (5)$$

respectively, where *i* stands for "initial", α is the isotope fractionation factor for hydrogen isotopes and *F* is the weight fraction of water remaining in the melt. It is worth noting that Eq. (4) and Eq. (5) apply to any kind of water-loss, notwithstanding if this occurs via decompression, degassing or dehydration upon CO_2-fluxing.

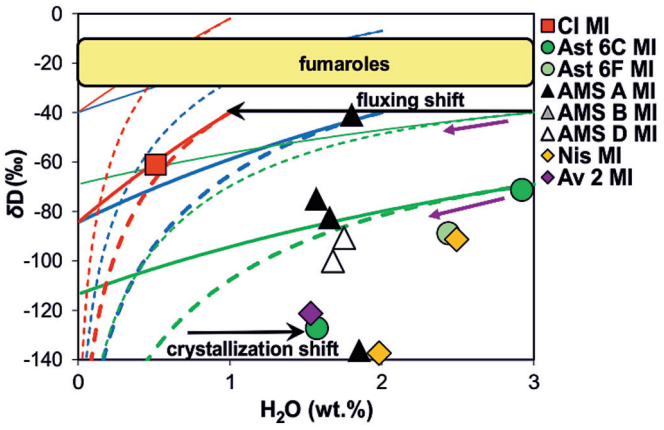

Fig. 10. H_2O (wt.%) vs. δD (‰) diagram. Composition of the analysed melt inclusions and calculated curves which model the evolution of the melt (thick, solid and dashed lines) and that of the associated gas phase (thin, solid and dashed lines) during both closed and open-system degassing regimes, respectively. Purple arrows indicate the direction of the degassing process. Curves with different colours have different H_2O and δD starting compositions (Green: H_2O = 3 wt.% and δD = –69‰; blue: H_2O = 2 wt.% and δD = –39.9‰; red: H_2O = 1 wt.% and δD = –39.9‰). The semi-transparent yellow field represents the present-day range of δD of the Campi Flegrei fumaroles (Caliro et al., 2007, 2025).

By using Eqs. (4) and (5) and the melt-vapour fractionation factor for hydrogen isotopes, we modelled the evolution of the melt during both closed and open-system degassing (thick, solid and dashed lines, respectively) as well as the evolution of the associated gas phase (thin, solid and dashed lines, respectively) which separates from the melt causing further fractionation (Fig. 10). Moreover, we investigated the role of CO_2 fluxing and crystallization in modifying the H_2O contents and δD values.

In order to explain the large variability of δD and the narrow range of H_2O in melt inclusions, we must first recall that the majority of the studied melt inclusions are not significantly affected by PEC and thus preserve their original chemical and isotopic signature. For calculations, we selected, as a starting point, one of the Astroni 6C melt inclusions. This melt inclusion was assumed to be representative of a relatively H_2O-rich melt, not modified by the arrival of a CO_2-rich gas, because it has the highest water content (2.9 wt.%) among the available data and displays a δD value of −71‰.

This value is similar to that of magmatic waters found in the Campi Flegrei boreholes (−46‰ to −79‰; Caprarelli et al., 1997) and to the values obtained on fluid inclusions entrapped in magmatic minerals, from the juvenile fraction of the 79 A.D. and 472 CE Vesuvius eruptions (Fulignati and Boyce, 2023). Fulignati and Boyce (2023) obtained δD values of the biotite between −52‰ and −58‰, and they interpret them as representative of the water dissolved in the melt, since it has been shown that there is little isotopic fractionation between OH-bearing minerals and melt water (Suzuoki and Epstein, 1976). The exact values used in our calculations as starting compositions (green curves in Fig. 10), are H_2O = 3 wt.% and δD = −69‰ for the magma (Supplementary Material 2, Supplementary Data Table S6). Based on the results of modelling, during evolution, the δD of the melt becomes more negative, i.e., moves from −69‰ to ~ −110‰ (Fig. 10), or even more negative in case of open-system degassing condition (dashed green curve in Fig. 10) while magma evolves and loses water from the liquid phase during degassing. Rightward shift from the curves, towards H_2O-rich terms, could be due to the crystallization that causes an increase of the dissolved H_2O content in the melt ("crystallization shift" arrow in Fig. 10), even if the whole system experiences water-loss. At the same time, due to isotope fractionation, the gas phase in equilibrium with the magma evolves displaying less negative δD than the melt (i.e., evolves from ~ −40‰ to ~ −70‰ or lighter in open-system degassing condition).

When fluxing occurs, the gas phase, characterized by less negative δD values (e.g., −70‰) with respect to the associated magma (−120‰), may re-equilibrate at shallower depth with a different melt. Fig. 10 shows that this melt (1) could be featured by lower H_2O contents (e.g., blue solid and dashed, thick lines), because the fluxing process is dominated by CO_2, and δD values of ~ −80‰; (2) could then acquire the less negative (−70‰) δD signature of the water vapor released by the deepest magma. This process is synthesized by the arrow labelled "fluxing shift" in Fig. 10, which connects the gas phase of a deep magma, having H_2O content = 3 wt.% and δD_i = ~ −40‰ (thin green lines), with a shallower (re-equilibrated) melt having H_2O contents of 2 wt.% (thick blue line). The shallower melt will be in equilibrium with a gas phase with less negative values of δD (thin blue lines) that can in turn intercept and react with an even more shallow magma, with even low H_2O contents (1 wt.% in Fig. 10, thick red line). However, Fig. 10 also shows a possible connection between the gas phase from the deep magma and the melt having 1 wt.% of H_2O contents. Consequently, each gas phase once flowing upward, may produce "fluxing shift arrays" in the uppermost levels of the vertically extended, transcrustal Campi Flegrei plumbing system. Along this system, different magma portions may re-equilibrate and then generate further closed and open-system degassing trends, also accompanied by magma crystallization. The chemical parameters were chosen as a simple example for describing a step-wise, cyclic process, acting during the evolution history of the Campi Flegrei volcanic area, including the bradyseismic crises. A similar process was described by Fulignati and Boyce (2023), for explaining the chemical and isotopic features of Vesuvius fluid inclusions. The occurrence of this process over time and at variable depths may have produced fluids with decreasing δD, reaching values in line with those reported in the present-day Campi Flegrei fumaroles (semi-transparent yellow field in Fig. 10; e.g., Caliro et al., 2007, 2025). The above mechanism brings to mind the chromatographic effect (Moretti et al., 2019), through which rising CO_2 and H_2O decouple, because CO_2 percolates faster due to its lower solubility with respect to H_2O. This partial decoupling favours the shallow magma to become enriched in a CO_2-rich, exsolved fluid phase and to acquire the hydrogen isotope signature of the gas rising from larger depth: in fact, when invested by early pulses of CO_2, magmas more efficiently dehydrate and acquire a less negative δD.

4.3. Reconstruction of the storage conditions and of the architecture of the plumbing system

The Campi Flegrei plumbing system has been reconstructed by many authors on the basis of petrological, geophysical and melt inclusions studies. Despite the differences among the proposed models, two main storage zones have been recognized: a deep reservoir filled by mafic, volatile-rich magmas at > ~170–200 MPa (Mangiacapra et al., 2008; Zollo et al., 2008; Arienzo et al., 2010, 2016; Moretti et al., 2013b; Fedi et al., 2018; Pappalardo and Buono, 2021; Buono et al., 2022; Caliro et al., 2025) and a relatively shallow felsic magma reservoir at < ~170–200 MPa (e.g., Arienzo et al., 2010, 2016; De Siena et al., 2010; Moretti et al., 2013b; Di Vito et al., 2016; Pappalardo and Buono, 2021; Buono et al., 2022). Equilibration pressures below 200 MPa, particularly below 100 MPa, were interpreted as shallow, transitory, short-lived magma apophyses (e.g., Balcone-Boissard et al., 2024, and references therein).

The majority of the melt inclusions analysed in this study record dissolved H_2O and CO_2 contents and trapping pressures in line with: (i) similar studies on Campi Flegrei melt inclusions (e.g., Signorelli et al., 2001; Roach, 2005; Cannatelli et al., 2007; Severs, 2007; Mangiacapra et al., 2008; Arienzo et al., 2010, 2016; Fourmentraux et al., 2012; Esposito et al., 2018; Voloschina et al., 2018), and (ii) crystallization and solubility experiments at variable pressures on Campi Flegrei products (Roach, 2005; Fanara et al., 2015; Supplementary Material 3, Supplementary Data Fig. S13). However, with respect to the experiments on the trachytic Campanian Ignimbrite samples (Fanara et al., 2015), the pressures calculated with the model of Papale et al. (2006) are ~50 to 100 MPa higher. This is likely due to the oxidation state at which the experiments were conducted (NNO + 2.6 log units), which is higher than that corresponding to the oxidation state assumed in this study by fixing Fe^{3+}/Fe_{tot} at 0.15 and 0.5. Additionally, the CO_2 contents measured by SIMS, although with large uncertainty (Esposito et al., 2014), are higher than literature values measured with Fourier Transform Infrared (FTIR) spectroscopy and in some cases could be underestimated in the melt inclusions with shrinkage bubbles.

The calculated entrapment pressures vary from 74 MPa to 645 MPa (or from 106 MPa to 564 MPa assuming a Fe^{3+}/Fe_{tot} ratio of 0.5). They were converted in depths using densities of 2.65 g/cm^3 for pressures less than 100 MPa, and of 2.90 g/cm^3 for pressures greater than 100 MPa, taking into account results of Fedi et al. (2018). The calculated depths vary from ~2.6 km to ~23 km.

The frequency histograms of the obtained pressures and depths (Fig. 11a and b) allow us to visualize the data distribution and how

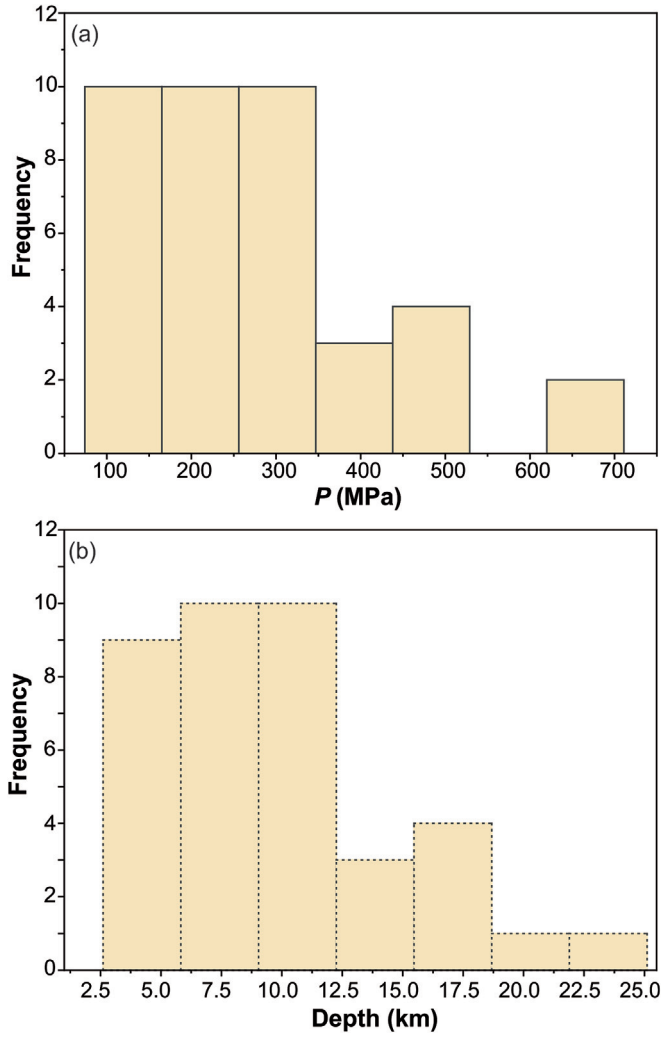

Fig. 11. Frequency histograms of the (a) pressures and (b) calculated depths. The bin width was calculated as follows: Bin Width $= \frac{\text{max\_value}-\text{min\_value}}{\text{N°analyses}^{-2}}$.

they are spread across different values. The histograms show that the frequency is similar for melt inclusions recording pressures between 74 MPa and 350 MPa, corresponding to depths from ~2.6 km to ~12.5 km. This crystallization/trapping depths range coincides with the location of the hypothesized felsic (shallowest) and mafic (deepest) Campi Flegrei reservoirs. However, eleven melt inclusions are featured by high pressures that converted in depth would suggest the unrealistic formation of trachytic magmas close to the local Moho, which is set at ~25–30 km depth (Di Stefano et al., 2011), below the Campi Flegrei volcanic area.

In order to constrain the meaning of these trapping pressures and of the associated storage depths, we combine the information retrieved by the solubility laws of the volatiles in melt inclusions with those obtained by the chemical composition of the investigated pyroxene. To this purpose, the distribution between Al^{IV} and Al^{VI} yields a first qualitative and reliable indication of their crystallization pressures. In fact, relatively low Al^{VI} can be considered typical of low-pressure crystallization conditions (e.g., Aoki and Kushiro, 1968; Aoki and Shiba, 1973; Thompson, 1974; Herzberg, 1978; Seyler and Bonatti, 1994). The pyroxene hosting the studied melt inclusions have Al^{IV} and Al^{VI} < 0.3 and 0.1, respectively. In Fig. 12, they are plotted together with experimentally produced pyroxenes (Laporte et al., 2014; Perinelli et al., 2019; Bonechi et al., 2021). Pyroxene in Laporte et al. (2014) was produced by experiments performed at 1000–1300 MPa and *T* of ~1200 °C, whereas pyroxene in Perinelli et al. (2019) through crystallization experiments performed at 800 MPa, and *T* of 1000–1310 °C. Pyroxene analysed by Bonechi et al. (2021) formed during crystallization experiments at 800 MPa and *T* of 1030–1250 °C. For comparison, the Al^{IV} and Al^{VI} of pyroxene from Astroni, Nisida, Averno 2, Campanian Ignimbrite and Agnano-Monte Spina from literature (Fedele et al., 2008; Arienzo et al., 2010, 2016; Fourmentraux et al., 2012) are also displayed. In addition, the coloured fields in Fig. 12 are built on the compositions of pyroxene produced in experiments at different pressures selected from the LEPR (Library of Experimental Phase Relations) database, following Perinelli et al. (2019). Both newly analysed and literature Campi Flegrei pyroxene have lower Al^{VI} with respect to the experimental pyroxenes falling in the fields of pressure higher than 0.5 GPa. Therefore, we may confidently assume that the crystallization pressure of the analysed pyroxene is lower than the calculated entrapment pressures at 500–650 MPa.

Specifically, Fig. 12 suggests that pyroxene likely crystallized in a pressure range from ~100 to ~300/500 MPa, therefore the highest pressures calculated with the model of Papale et al. (2006) are overestimated. This hypothesis is corroborated by the pressure estimates obtained by Pelullo et al. (2022b) on clinopyroxene from Agnano-Monte Spina having Mg# = 70–78 (in the same range of clinopyroxene analysed in this study) which yielded values of 30–240 MPa. By assuming that variations in the oxidation state likely occur during magma crystallization and transfer from the deepest part of the feeding system (>200 MPa) up to the surface (see Section 4.2.1), Fe^{3+}/Fe_{tot} = 0.5 better reproduces the features of the magmas at pressures greater than 200 MPa. This ratio produces slightly lower entrapment pressures not exceeding 564 MPa (Supplementary Material 2, Supplementary Data Table S2), in agreement with the experiments presented in Fanara et al. (2015) (Supplementary Material 3, Supplementary Data Fig. S13). However, the different redox condition alone does not completely explain the meaning of the high pressures, trachytic melt inclusions. More likely, the pressure estimates above ~ 300 MPa could be explained by local overpressure, induced by gas fluxing, occurring at variable depths, which adds to the lithostatic pressure, leading to the increase in the saturation pressure recorded by melt inclusions, which cannot be simply converted into lithostatic pressures over the crystallizing melt. Notwithstanding this limitation, our results are extremely important for the comprehension of the architecture and processes acting in the Campi Flegrei feeding system. In fact, for the first time, we are emphasizing the importance of the occurrence of relatively evolved magmas at pressure ≥ 200 MPa, suggesting the temporary coexistence of felsic magma batches in a deep mafic magma reservoir (Fig. 13). Evidences of storage at large depth of trachytic magmas were already presented for high magnitude eruptions such as the Campanian Ignimbrite, the Neapolitan Yellow Tuff, and the Agnano-Monte Spina eruptions, for which pressures up to 500 MPa were calculated (Roach, 2005; Arienzo et al., 2010; Esposito et al., 2018; Moretti et al., 2019). An important consequence is that the presence of evolved magmas at depth larger than 200 MPa may have influence on the temperatures and density distribution, and on the stability of the feeding system. Once formed due to crystallization induced by fluxing, the felsic magma batches, becoming unstable and buoyant, can easily find a pathway to the surface, sustained by the large amount of volatiles that separate and accumulate at shallow depth (above 200 MPa). This process might also induce mixing among magmas with different compositions, explaining several hybrid features, including mineralogic and isotopic disequilibria, displayed by many Campi Flegrei rocks, especially from recent eruptions (e.g., Tonarini et al., 2009;

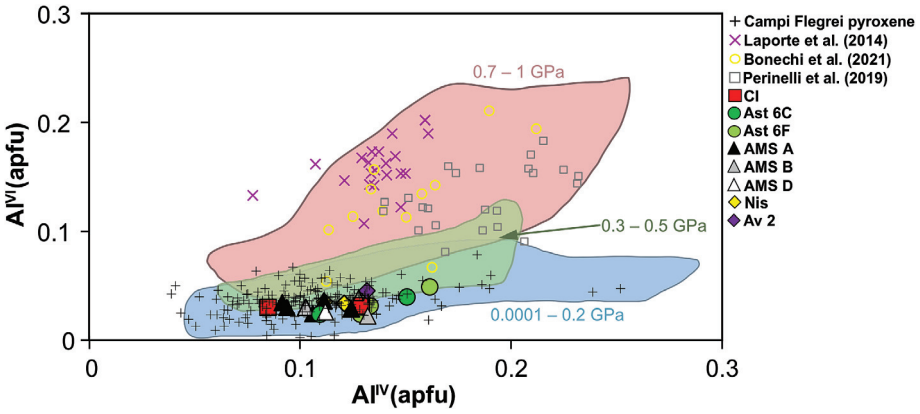

Fig. 12. Al^{IV} (apfu) vs. Al^{VI} (apfu) variation diagram. Al^{IV} apfu = 2 –Si apfu; Al^{VI}apfu = (6/anion sum) × cations of Al^{tot} –Al^{IV} (apfu). Coloured fields are from LEPR database (Perinelli et al., 2019). The red one includes experiments carried out at 0.7–1 GPa, the green one experiments carried out at 0.3–0.5 GPa and the blue one experiments from 0.0001 and 0.2 GPa. Experiments on pyroxene were carried out by Laporte et al. (2014), using rocks from the Massif Central, at 1000–1300 MPa, and by Perinelli et al. (2019) and Bonechi et al. (2021), using rocks from Procida, at 800 MPa. Campi Flegrei literature data are on pyroxene from: Astroni (Arienzo et al., 2016); Nisida (Arienzo et al., 2016); Averno 2 (Fourmentraux et al., 2012); Campanian Ignimbrite (Fedele et al., 2008); Agnano-Monte Spina (Arienzo et al., 2010).

Di Renzo et al., 2011; Arienzo et al., 2016; D'Antonio et al., 2022, and references therein).

Remarkably, for some of the studied eruptions, melt inclusions align along Curve 0 in Fig. 8a, which has a constant proportion of H_2O (10 mol%) and CO_2 (90 mol%), or along a CO_2 richer curve (not shown) where Agnano Monte-Spina and Campanian Ignimbrite melt inclusions seem to be aligned. This may indicate that, in those specific cases, corresponding to high magnitude eruptions, the magma transfer was dominated by a CO_2-rich gas phase in equilibrium with the magma.

Following a mechanism previously suggested by Moretti et al. (2013b) and that with different nuances was also suggested by De Vivo and Lima (2006), Bodnar et al. (2007), Lima et al. (2009, 2021) and Caliro et al. (2025), the principal actor of the bradyseismic crises, particularly after the 2005–2012, is possibly the deep system (> 200 MPa) which is degassing and consequently transferring gas to the system between 200 MPa and 100 MPa (~8 km to ~4 km) and in turn to the uppermost hydrothermal system. Magma ascent has been proposed for the actual bradiseismic crises by Astort et al. (2024) and Giacomuzzi et al. (2024), whereas Moretti et al. (2013b, 2018b)) and Caliro et al. (2025) proposed, for the actual crises, that the uplift episodes were mostly driven by deep fluid influx in the aquifers.

Whatever process is in place today, the arrival of gas, possibly from just above the local Moho, in the deep portions of the transcrustal Campi Flegrei plumbing system (~200–350 MPa) and the consequent formation of trachytic magma batches may favour fracturing of a crystal-rich/fragile zone (see Fig. 13) and earthquakes at ~9–10 km depth (e.g. earthquake of 2025/04/13, 05:37:55, local time; in https://terremoti.ov.ingv.it/gossip/flegrei/index.html, access 14 April 2025). It may also induce pressurization of the shallow part of the Campi Flegrei caldera, up to the base of the hydrothermal system causing the majority of the earthquakes and seismic swarms, which are located between ~1–4 km depth. These processes may cause instability, possibly facilitating magma ascent and interconnection among the deepest and the shallowest portions of the plumbing system, and then the eruptions.

As already suggested by Arienzo et al. (2010) and Moretti et al (2018b), the connection among different portions of the plumbing system could be favoured by depressurization induced by the possible disruption of the cap of rocks below the hydrothermal system, weakened by the continuous supply of deep gas, particularly CO_2, into the shallow zones. The depressurization may facilitate the emptying of uppermost, small, short-living reservoirs, and the consequent transfer of magma from the > 200 MPa deep regions, upward. This process may possibly escalate towards a high magnitude eruption at high XCO_2 gas value (~0.9; e.g., Agnano Monte Spina, Campanian Ignimbrite). This composition, if detected during the geochemical monitoring of the fumaroles, may suggest the arrival of deep magmas. However, such high XCO_2 gas value could be not necessarily detected due to the possible occurrence of events producing a too fast depressurization (e.g., phreatic eruptions, earthquakes). In addition, the proposed scenario explains why the majority of magmas drawn toward the surface are not mafic; conversely, in agreement with volcanological and geochemical reconstructions, in most of the cases they are felsic, CO_2 rich magmas, easier to mobilize.

5. Conclusions

For active volcanoes, such as the Campi Flegrei volcanic field, the knowledge of the architecture of the plumbing system and the processes favouring or triggering the variable magnitude eruptions are extremely important for the land use management in case of volcanic crises, such as the current unrest phase. Therefore, it is important to deepen the knowledge on the geochemical features of the magma feeding past eruptions and on the pre- and syn-eruptive magmatic processes that can affect the eruptive dynamics.

Our combined microanalytical study on pyroxene-hosted melt inclusions from different Campi Flegrei eruptions allow us to identify a major crystallization zone located at an equivalent depth from ~2.6 km to ~12.5 km. Major points, which emerge from our study, are:

(1) Papale et al. (2006) model returns entrapment pressures between 74 MPa and 645 MPa, which cannot be simply converted into lithostatic pressures over the crystallizing melt. Our data suggest that melt inclusions may record local overpressure, due to the presence of a gas phase in equilibrium with the uprising and crystallizing magma. Local overpressures due to CO_2 fluxing may affect the calculated trapping pressures below the fragile-ductile transition.

(2) Between ~100 MPa and < 300 MPa, possibly at Fe^{3+}/Fe_{tot} = 0.15, relatively evolved trachytic magmas form and may accumulate.

(3) At pressure > 250–300 MPa, at Fe^{3+}/Fe_{tot} = 0.15 or even at Fe^{3+}/Fe_{tot} = 0.5, trachytic magmas may temporarily coexist with

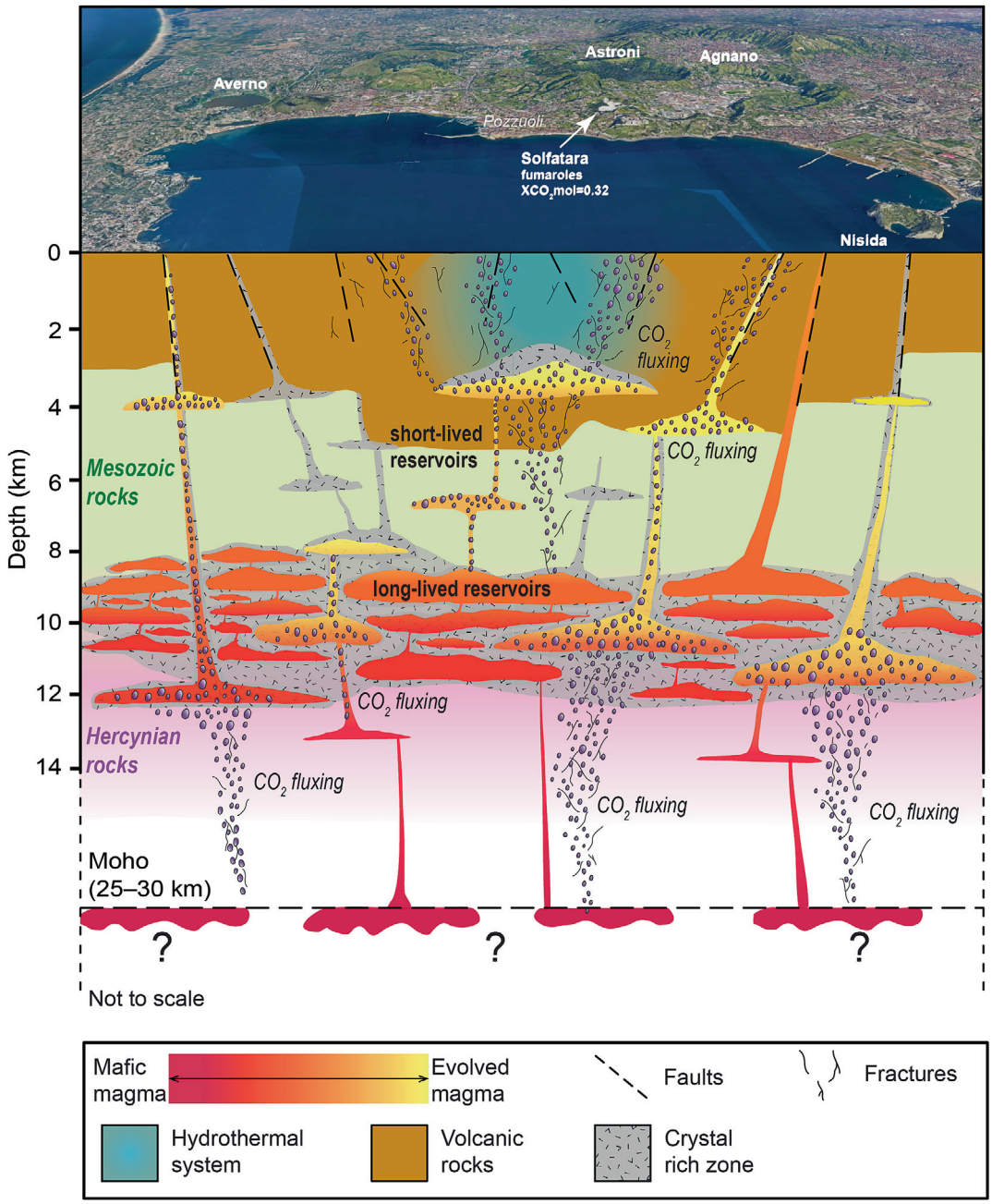

Fig. 13. Sketch illustrating the Campi Flegrei plumbing system architecture and processes, as reconstructed by solubility models of volatile contents in melt inclusions, clinopyroxene compositions and previous knowledge. The sketch shows the coexistence of felsic and mafic batches in the deep system (>8 km) and connection between the deep and shallow storage zones (that can occur before/during eruption). The volatile fluxing drives the evolution of mafic magmas toward trachytic to phonolitic composition and causes overpressure, able to give rise to highly explosive eruptions. The Moho depth and the rocks of the basement are from Di Stefano et al. (2011) and Pappalardo and Mastrolorenzo (2012).

relatively less evolved magmas. When the deep-seated trachytic magma batches, containing up to 5–6 wt.% of total dissolved gases, reach a critical volume with respect to the surrounding mafic magmas, and equilibrate with a volatile rich gas phase extremely rich in CO_2 (75–90 mol%), they become highly buoyant. This process may lead to magma ascent, and further crystallization and degassing at shallow depth. Furthermore, the coexistence of mafic and felsic magmas may generate hybrid magmas of which there is evidence in several, especially young, Campi Flegrei eruptive products.

(4) The appropriate choice of total volatile contents (H_2O^T, CO_2^T, S^T) and redox state generates degassing paths that in combination with crystallization and fluxing may explain the ensemble of melt inclusions data.

(5) Results of modelling support the concept that the Campi Flegrei plumbing system acts like a crustal magmatic chromatograph, which produces CO_2-rich gas flooding the shallowest part of the feeding system (Moretti et al., 2019).

(6) Our modelling suggests that the δD of the melt becomes more negative while magma evolves and loses water from the liquid phase during degassing. A shift towards H_2O-rich terms could be due to crystallization that causes an increase of the dissolved H_2O content in the melt. At the same time, due to isotope fractionation, the gas phase in equilibrium with the magma evolves dis-

playing less negative δD than the melt, approaching the δD of the local magmatic water discharged from present-day fumaroles. Although we cannot exclude that few melt inclusions were affected by H_2O loss due to diffusion, or other post-entrapment processes, we have no clear evidence for this occurrence. In any case, this possibility will not invalid the fluxing hypothesis and the general interpretation of the dynamic and architecture of the Campi Flegrei plumbing system.

(7) The Agnano Monte-Spina eruption displays the largest overpressure, with respect to the other recent eruptions. Therefore, a relation between local overpressure and explosivity of the eruptions can be suggested. It implies the occurrence, in most cases, of a CO_2 rich-gas phase associated to the eruptible magma.

(8) Extreme values in our dataset (e.g., H_2O ~0.5 wt.% for the Campanian Ignimbrite melt inclusions) might be explained by H-loss or by introducing one more set of total volatile contents, even more enriched in CO_2 that could be related to an extremely fluxed and dehydrated magma. It is not by chance that the Campanian Ignimbrite eruption was the most explosive event of the Mediterranean area.

(9) Our data strengthen that before/during volcanic activity at Campi Flegrei a sequence of events and processes (e.g., fluxing, crystallization) may have occurred several times and at variable depths, producing magmas with chemical features similar to those recorded by melt inclusions, and gases with the chemical features of gases from the Solfatara fumaroles.

(10) Finally, our reconstruction also implies that the entire crust beneath Campi Flegrei is flooded by huge amounts of magmatic fluids, possibly produced close to the local Moho that migrate to the surface explaining the high CO_2 content of melt inclusions, the occurrence of gas rich zones below the hydrothermal system and the strong CO_2 emissions observed at surface.

CRediT authorship contribution statement

Ilenia Arienzo: Writing – review & editing, Writing – original draft, Validation, Project administration, Investigation, Funding acquisition, Formal analysis, Data curation, Conceptualization. **Bruna Cariddi:** Writing – review & editing, Visualization, Validation, Data curation, Conceptualization. **Carlo Pelullo:** Writing – review & editing, Visualization, Validation. **Claudia D'Oriano:** Writing – review & editing, Validation, Investigation, Formal analysis, Data curation. **Etienne Deloule:** Writing – review & editing, Visualization, Investigation, Formal analysis, Data curation. **Massimo D'Antonio:** Writing – review & editing, Validation, Conceptualization. **Roberto Moretti:** Writing – review & editing, Writing – original draft, Validation, Software, Formal analysis, Data curation, Conceptualization.

Declaration of competing interest

The authors declare that they have no known competing financial interests or personal relationships that could have appeared to influence the work reported in this paper.

Acknowledgments

The authors kindly thank the Associate Editor Mathew Domeier, Prof. Rosario Esposito and an anonymous reviewer for their constructive criticism and suggestions. G. Orsi, L. Civetta and Girolamo Milano are kindly thanked for useful suggestions and discussions during the period of data acquisition and processing. The authors thank the colleagues from the INGV, Osservatorio Vesuviano Administrative Services for their valuable contribution to the research. The INGV-OV laboratories have been financially supported by the EPOS Research Infrastructure through the contribution of the Italian Ministry of University and Research (MUR). This work benefit of the financial support from the Istituto Nazionale di Geofisica e Vulcanologia, Italy, grant "Progetto INGV Pianeta Dinamico" — code CUP D53J19000170001 — funded by Italian Ministry MIUR ("Fondo Finalizzato al rilancio degli investimenti delle amministrazioni centrali dello Stato e allo sviluppo del Paese," legge 145/2018)", sub-project SMEEGOL (Resp. Ilenia Arienzo).

Appendix A. Supplementary data

Supplementary data to this article can be found online at https://doi.org/10.1016/j.gsf.2026.102262.

References

Aiuppa, A., Moretti, R., Federico, C., Giudice, G., Gurrieri, S., Liuzzo, M., Papale, P., Shinohara, H., Valenza, M., 2007. Forecasting Etna eruptions by real-time observation of volcanic gas composition. Geology 35, 1115–1118. https://doi.org/10.1130/G24149A.1.

Aiuppa, A., Cannata, A., Cannavò, F., Di Grazia, G., Ferrari, F., Giudice, G., Gurrieri, S., Liuzzo, M., Mattia, M., Montalto, P., Patanè, D., Puglisi, G., 2010. Patterns in the recent 2007–2008 activity of Mount Etna volcano investigated by integrated geophysical and geochemical observations. Geochem. Geophys. Geosyst. 11, Q09008. https://doi.org/10.1029/2010GC003168.

Aiuppa, A., Bitetto, M., Calabrese, S., Delle Donne, D., Lages, J., La Monica, F.P., Chiodini, G., Tamburello, G., Cotterill, A., Fulignati, P., Gioncada, A., Liu, E.J., Moretti, R., Pistolesi, M., 2022. Mafic magma feeds degassing unrest at Vulcano Island, Italy. Commun. Earth Environ. 3, 255. https://doi.org/10.1038/s43247-022-00589-1.

Anders, E., Grevesse, N., 1989. Abundances of the elements: meteoritic and solar. Geochim. Cosmochim. Acta 53, 197–214. https://doi.org/10.1016/0016-7037(89)90286-X.

Aoki, K.I., Kushiro, I., 1968. Some clinopyroxenes from ultramafic inclusions in Dreiser Weiher. Eifel. Contr. Mineral. Petrol. 18, 326–337. https://doi.org/10.1007/BF00399694.

Aoki, K.I., Shiba, I., 1973. Pyroxenes from lherzolite inclusions of Itinome-gata, Japan. Lithos 6, 41–51. https://doi.org/10.1016/0024-4937(73)90078-9.

Arienzo, I., Moretti, R., Civetta, L., Orsi, G., Papale, P., 2010. The feeding system of Agnano-Monte Spina eruption (Campi Flegrei, Italy): dragging the past into the present activity and future scenarios. Chem. Geol. 270, 135–147. https://doi.org/10.1016/j.chemgeo.2009.11.012.

Arienzo, I., Cariddi, B., Pelullo, C., D'Oriano, C., Deloule, E., D'Antonio, M., Moretti, R., 2026. Micro-analytical investigations on Campi Flegrei pyroxene-hosted melt inclusions, H_2O-CO_2-S-melt and δD modelling. Mendeley Data V3. https://doi.org/10.17632/5725jzvwbx.2.

Arienzo, I., Mazzeo, F.C., Moretti, R., Cavallo, A., D'Antonio, M., 2016. Open system magma evolution and fluid transfer at Campi Flegrei caldera (Southern Italy) during the past 5 ka as revealed by geochemical and isotopic data: the example of the Nisida eruption. Chem. Geol. 427, 109–124. https://doi.org/10.1016/j.chemgeo.2016.02.007.

Astort, A., Trasatti, E., Caricchi, L., Polcari, M., De Martino, P., Acocella, V., y Di Vito, M.A., 2024. Tracking the 2007–2023 magma-driven unrest at Campi Flegrei caldera (Italy). Commun. Earth Environ. 5 (1), 506. https://doi.org/10.1038/s43247-024-01665-4.

Balcone-Boissard, H., Boudon, G., d'Augustin, T., Erdmann, S., Deloule, E., Vicente, J., 2023. Architecture of the Lesser Antilles arc illustrated by melt inclusions. J. Petrol. 64, egad020. https://doi.org/10.1093/petrology/egad020.

Balcone-Boissard, H., Boudon, G., Zdanowicz, G., Orsi, G., Webster, J.D., Civetta, L., D'Antonio, M., Arienzo, I., 2024. The space-time architecture variation of the shallow magmatic plumbing systems feeding the Campi Flegrei and Ischia volcanoes (Southern Italy) from halogen constraints. Am. Miner. 109, 977–991. https://doi.org/10.2138/am-2022-8883.

Barth, A., Plank, T., 2021. The ins and outs of water in olivine-hosted melt inclusions: hygrometer vs. speedometer. Front. Earth Sci. 9, 614004. https://doi.org/10.3389/feart.2021.614004.

Bevilacqua, A., Isaia, R., Neri, A., Vitale, S., Aspinall, W.P., Bisson, M., Flandoli, F., Baxter, P.J., Bertagnini, A., Esposti Ongaro, T., Iannuzzi, E., Pistolesi, M., Rosi, M., 2015. Quantifying volcanic hazard at Campi Flegrei caldera (Italy) with uncertainty assessment: 1. Vent opening maps. J. Geophys. Res.: Sol. Earth 120, 2309–2329. https://doi.org/10.1002/2014JB011776.

Blundy, J., Cashman, K., 2008. Petrologic reconstruction of magmatic systems variables and processes. Rev. Mineral. Geochem. 69, 179–239. https://doi.org/10.2138/rmg.2008.69.6.

Bodnar, R.J., Cannatelli, C., De Vivo, B., Lima, A.M., Belkin, H.E., Milia, A., 2007. Quantitative models for magma degassing and ground deformation (bradyseism) at Campi Flegrei, Italy: Implications for future eruptions. Geology 35, 791–794. https://doi.org/10.1130/G23653A.1.

Bonechi, B., Perinelli, C., Gaeta, M., Fabbrizio, A., Petrelli, M., Strnad, L., 2021. High pressure trace element partitioning between clinopyroxene and alkali basaltic melts. Geochim. Cosmochim. Acta 305, 282–305. https://doi.org/10.1016/j.gca.2021.04.023.

Branca, S., Cinquegrani, A., Cioni, R., Conte, A.M., Conticelli, S., De Astis, G., de Vita, S., De Rosa, R., Di Vito, M.A., Donato, P., Forni, F., Francalanci, L., Gaeta, M., Giaccio, B., Giordano, G., Giuffrida, M., Isaia, R., Lucchi, F., Marra, F., Massaro, S., Nicotra, E., Palladino, D.M., Perinelli, C., Petrosino, P., Pistolesi, M., Romagnoli, C., Rotolo, S., Sottili, G., Sulpizio, R., Tranne, C.A., Viccaro, M., 2023. The Italian Quaternary volcanism. Alp. Mediterr. Quat. 36 (1131), 221–284.

Buono, G., Paonita, A., Pappalardo, L., Caliro, S., Tramelli, A., Chiodini, G., 2022. New insights into the recent magma dynamics under Campi Flegrei caldera (Italy) from petrological and geochemical evidence. J. Geophys. Res. Solid Earth 127, e2021JB023773. https://doi.org/10.1029/2021JB023773.

Burton, M., Aiuppa, A., Allard, P., Asensio-Ramos, M., Pardo Cofrades, A., La Spina, A., Nicholson, E.J., Zanon, V., Barrancos, J., Bitetto, M., Hartley, M., Romero, J.E., Waters, E., Stewart, A., Hernández, P.A., Pedro Lages, J., Padrón, E., Wood, K., Esse, B., Hayer, C., Cyrzan, K., Rose-Koga, E.F., Schiavi, F., D'Auria, L., Pérez, N.M., 2023. Exceptional eruptive CO_2 emissions from intra-plate alkaline magmatism in the Canary volcanic archipelago. Commun. Earth Environ. 4, 467.

Caliro, S., Chiodini, G., Moretti, R., Avino, R., Granieri, D., Russo, M., Fiebig, J., 2007. The origin of the fumaroles of La Solfatara (Campi Flegrei, South Italy). Geochim. Cosmochim. Acta 71, 3040–3055. https://doi.org/10.1016/j.gca.2007.04.007.

Caliro, S., Chiodini, G., Avino, R., Carandente, A., Cuoco, E., Di Vito, M.A., Minopoli, C., Rufino, F., Santi, A., Lages, J., Mangiacapra, A., Monteleone, B., Pappalardo, L., Taracsák, Z., Tramati, C., Vizzini, S., Aiuppa, A., 2025. Escalation of caldera unrest indicated by increasing emission of isotopically light sulfur. Nat. Geosci. 18, 167–174. https://doi.org/10.1038/s41561-024-01632-w.

Cannatelli, C., Lima, A., Bodnar, R.J., De Vivo, B., Webster, J.D., Fedele, L., 2007. Geochemistry of melt inclusions from the Fondo Riccio and Minopoli 1 eruptions at Campi Flegrei (Italy). Chem. Geol. 237, 418–432. https://doi.org/10.1016/j.chemgeo.2006.07.012.

Caliro, S., Chiodini, G., Paonita, A., 2014. Geochemical evidences of magma dynamics at Campi Flegrei (Italy). Geochim. Cosmochim. Acta 132, 1–15. https://doi.org/10.1016/j.gca.2014.01.021.

Cannatelli, C., Doherty, A.L., Esposito, R., Lima, A., De Vivo, B., 2016. Understanding a volcano through a droplet: a melt inclusion approach. J. Geochem. Explor. 171, 4–19. https://doi.org/10.1016/j.gexplo.2015.10.003.

Caprarelli, G., Tsutsumi, M., Turi, B., 1997. Chemical and isotopic signatures of the basement rocks from the Campi Flegrei geothermal field (Naples, southern Italy): inferences about the origin and evolution of its hydrothermal fluids. J. Volcanol. Geotherm. Res. 76, 63–82. https://doi.org/10.1016/S0377-0273(96)00072-8.

Capriolo, M., Marzoli, A., Aradi, L.E., Callegaro, Sara, Dal Corso, Jacopo, Newton, R.J., Mills, B. J.W., Wignall P.B., Bartoli, O., Don R. Baker, Youbi N., Remusat, L., Spiess R., Szabó, C., 2020. Deep CO_2 in the end-Triassic central Atlantic magmatic province. Nat. Commun. 11, 1670. https://doi.org/10.1038/s41467-020-15325-6.

Caricchi, L., Montagna, C.P., Aiuppa, A., Lages, J., Tamburello, G., Papale, P., 2024. CO_2 flushing triggers paroxysmal eruptions at open conduit basaltic volcanoes. J. Geophys. Res.: Sol. Earth 129, e2023JB028486. https://doi.org/10.1029/2023JB028486.

Caricchi, L., Sheldrake, T.E., Blundy, J., 2018. Modulation of magmatic processes by CO_2 flushing. Earth Planet. Sci. Lett. 491, 160–171. https://doi.org/10.1016/j.epsl.2018.03.042.

Cariddi, B., Maingault, L., De Hoog, J., Pelullo, C., Arienzo, I., 2026. Major and volatile elements contents in clinopyroxene-hosted melt inclusions from Campi Flegrei eruptions. Mendeley Data V1.

Chiodini, G., Caliro, S., Avino, R., Bagnato, E., Capecchiacci, F., Carandente, A., Cardellini, C., Minopoli, C., Tamburello, G., Tripaldi, S., Aiuppa, A., 2022. The hydrothermal system of the Campi Flegrei caldera, Italy. In: Orsi, G., D'Antonio, M., Civetta, L. (Eds.), Campi Flegrei. Active Volcanoes of the World. Springer, Berlin, Heidelberg, pp. 239–255. https://doi.org/10.1007/978-3-642-37060-1_9.

Civetta, L., Orsi, G., Pappalardo, L., Fisher, R.V., Heiken, G., Ort, M., 1997. Geochemical zoning, mingling, eruptive dynamics and depositional processes – the Campanian ignimbrite, Campi Flegrei caldera, Italy. J. Volcanol. Geotherm. Res. 75, 183–219.

D'Antonio, M., Arienzo, I., Di Renzo, V., Civetta, L., Carandente, A., Tonarini, S., 2022. Origin and differentiation history of the magmatic system feeding the Campi Flegrei volcanic field (Italy) constrained by radiogenic and stable isotope data. In: Orsi, G., D'Antonio, M., Civetta, L. (Eds.), Campi Flegrei: a Restless Caldera in a Densely Populated Area. Springer, Berlin, Heidelberg, pp. 125–149. https://doi.org/10.1007/978-3-642-37060-1_4.

D'Antonio, M., Civetta, L., Orsi, G., Pappalardo, L., Piochi, M., Carandente, A., de Vita, S., Di Vito, Isaia, R., 1999. The present state of the magmatic system of the Campi Flegrei caldera based on a reconstruction of its behaviour in the past 12 ka. J. Volcanol. Geotherm. Res. 91, 247–268. https://doi.org/10.1016/S0377-0273(99)00038-4.

Danyushevsky, L.V., McNeill, A.W., Sobolev, A.V., 2002. Experimental and petrological studies of melt inclusions in phenocrysts from mantle-derived magmas: an overview of techniques, advantages and complications. Chem. Geol. 183, 5–24. https://doi.org/10.1016/S0009-2541(01)00369-2.

De Hoog, J.C., Taylor, B.E., Van Bergen, M.J., 2009. Hydrogen-isotope systematics in degassing basaltic magma and application to Indonesian arc basalts. Chem. Geol. 266, 256–266. https://doi.org/10.1016/j.chemgeo.2009.06.010.

De Martino, P., Dolce, M., Brandi, G., Scarpato, G., Tammaro, U., 2021. The ground deformation history of the Neapolitan volcanic area (Campi Flegrei caldera, Somma–Vesuvius volcano, and Ischia island) from 20 years of continuous GPS observations (2000–2019). Remote Sens. 13, 2725. https://doi.org/10.3390/rs13142725.

De Siena, L., Del Pezzo, E., Bianco, F., 2010. Seismic attenuation imaging of Campi Flegrei: evidence of gas reservoirs, hydrothermal basins, and feeding systems. J. Geophys. Res.: Sol. Earth 115, B09312. https://doi.org/10.1029/2009JB006938.

de Vita, S., Orsi, G., Civetta, L., Carandente, A., D'Antonio, M., Deino, A., di Cesare, T., Di Vito, M.A., Fisher, R.V., Isaia, R., Marotta, E., Necco, A., Ort, M., Pappalardo, L., Piochi, M., Southon, J., 1999. The Agnano–Monte Spina eruption (4100 years BP) in the restless Campi Flegrei caldera (Italy). J. Volcanol. Geotherm. Res. 91, 269–301. https://doi.org/10.1016/S0377-0273(99)00039-6.

Del Gaudio, C., Aquino, I., Ricciardi, G.P., Ricco, C., Scandone, R., 2010. Unrest episodes at Campi Flegrei: a reconstruction of vertical ground movements during 1905–2009. J. Volcanol. Geotherm. Res. 195, 48–56. https://doi.org/10.1016/j.jvolgeores.2010.05.014.

De Natale, G., Troise, C., Mark, D., Mormone, A., Piochi, M., Di Vito, M.A., Isaia, R., Carlino, S., Barra, D., Somma, R., 2016. The Campi Flegrei Deep Drilling Project (CFDDP): New insight on caldera structure, evolution and hazard implications for the Naples area (Southern Italy). Geochem. Geophys. Geosyst. 17 (12), 4836–4847. https://doi.org/10.1002/2015gc006183.

De Vivo, B., Lima, A., 2006. Chapter 14 A hydrothermal model for ground movements (bradyseism) at Campi Flegrei, Italy. In: De Vivo, B. (Ed.), Developments in Volcanology, 9. Elsevier, Amsterdam, pp. 289–317. https://doi.org/10.1016/S1871-644X(06)80028-8.

De Vivo, B., Rolandi, G., Gans, P.B., Calvert, A., Bohrson, W.A., Spera, F.J., Belkin, H.E., 2001. New constrains of pyroclastic eruptive history of the Campanian Volcanic Plain. Mineral. Petrol. 73, 47–65. https://doi.org/10.1007/s007100170010.

Di Muro, A., Mètrich, N., Vergani, D., Rosi, M., Armienti, P., Fourgeroux, T., Deloule, E., Arienzo, I., Civetta, L., 2014. The shallow plumbing system of Piton de la Fournaise Volcano (La Réunion island, Indian Ocean) revealed by the major 2007 caldera forming eruption. J. Petrol. 55, 1287–1315. https://doi.org/10.1093/petrology/egu025.

Di Renzo, V., Arienzo, I., Civetta, L., D'Antonio, M., Tonarini, S., Di Vito, M.A., Orsi, G., 2011. The magmatic feeding system of the Campi Flegrei caldera: architecture and temporal evolution. Chem. Geol. 281, 227–241. https://doi.org/10.1016/j.chemgeo.2010.12.010.

Di Stefano, R., Bianchi, I., Ciaccio, M.G., Carrara, G., Kissling, E., 2011. Three-dimensional Moho topography in Italy: new constraints from receiver functions and controlled source seismology. Geochem. Geophys. Geosyst. 12, Q09006. https://doi.org/10.1029/2011GC003649.

Di Vito, M.A., Arienzo, I., Braia, G., Civetta, L., D'Antonio, M., Orsi, G., 2011. The Averno 2 fissure eruption: a recent small size explosive event at the Campi Flegrei caldera. Bull. Volcanol. 73, 295–320. https://doi.org/10.1007/s00445-010-0417-0.

Di Vito, M.A., Acocella, V., Aiello, G., Barra, D., Battaglia, M., Carandente, A., Del Gaudio, C., de Vita, S., Ricciardi, G.P., Ricco, C., Scandone, R., Terrasi, F., 2016. Magma transfer at Campi Flegrei caldera (Italy) before the 1538 AD eruption. Sci. Rep. 6, 32245. https://doi.org/10.1038/srep32245.

Edmonds, M., Aiuppa, A., Humphreys, M., Moretti, R., Giudice, G., Martin, R.S., Herd, R.A., Christopher, T., 2010. Excess volatiles supplied by mingling of mafic magma at an andesite arc volcano. Geochem. Geophys. Geosyst. 11, Q04005. https://doi.org/10.1029/2009GC002781.

Esposito, R., Bodnar, R.J., Danyushevsky, L.V., De Vivo, B., Fedele, L., Hunter, J., Lima, A., Shimizu, N., 2011. Volatile evolution of magma associated with the Solchiaro eruption in the Phlegrean Volcanic District (Italy). J. Petrol. 52, 2431–2460. https://doi.org/10.1093/petrology/egr051.

Esposito, R., Hunter, J., Schiffbauer, J.D., Shimizu, N., Bodnar, R.J., 2014. An assessment of the reliability of melt inclusions as recorders of the pre-eruptive volatile content of magmas. Am. Mineral. 99, 976–998.

Esposito, R., Lamadrid, H.M., Redi, D., Steele-MacInnis, M., Bodnar, R.J., Manning, C. E., De Vivo, B., Cannatelli, C., Lima, A., 2016. Detection of liquid H_2O in vapor bubbles in reheated melt inclusions: Implications for magmatic fluid composition and volatile budgets of magmas? Am. Mineral. 101, 1691–1695. https://doi.org/10.2138/am-2016-5689.

Esposito, R., 2020. Magmatism of the Phlegrean Volcanic Fields as revealed by melt inclusions. In: De Vivo, B., Belkin, H.E., Rolandi, G. (Eds.), Vesuvius, Campi Flegrei, and Campanian Volcanism. Elsevier, pp. 141–174. https://doi.org/10.1016/B978-0-12-816454-9.00007-9.

Esposito, R., Badescu, K., Steele-MacInnis, M., Cannatelli, C., De Vivo, B., Lima, A., Bodnar, R., Manning, C.E., 2018. Magmatic evolution of the Campi Flegrei and Procida volcanic fields, Italy, based on interpretation of data from well-constrained melt inclusions. Earth Sci. Rev. 185, 325–356 https://hdl.handle.net/10281/348488.

Esposito, R., Redi, D., Danyushevsky, L.V., Gurenko, A., de Vivo, B., Manning, C.E., Bodnar, R.J., Steele-MacInnis, M., Frezzotti, M.L., 2023. Constraining the volatile evolution of mafic melts at Mt. Somma–Vesuvius, Italy, based on the composition of reheated melt inclusions and their olivine hosts. Eur. J. Mineral. 35, 921–948. https://doi.org/10.5194/ejm-35-921-2023.

Fanara, S., Botcharnikov, R.E., Palladino, D.M., Adams, F., Buddensieck, J., Mulch, A., Behrens, H., 2015. Volatiles in magmas related to the Campanian ignimbrite eruption: Experiments vs. natural findings. Am. Miner. 100, 2284–2297. https://doi.org/10.2138/am-2015-5033.

Fedele, L., Scarpati, C., Lanphere, M., Melluso, L., Morra, V., Perrotta, A., Ricci, G., 2008. The Breccia Museo formation, Campi Flegrei, southern Italy:

geochronology, chemostratigraphy and relationship with the Campanian ignimbrite eruption. Bull. Volcanol. 70, 1189–1219. https://doi.org/10.1007/s00445-008-0197-y.
Fedele, L., Zanetti, A., Morra, V., Lustrino, M., Melluso, L., Vannucci, R., 2009. Clinopyroxene/liquid trace element partitioning in natural trachyte–trachyphonolite systems: insights from Campi Flegrei (southern Italy). Contrib. Mineral. Petrol. 158, 337–356. https://doi.org/10.1007/s00410-009-0386-5.
Fedi, M., Cella, F., D'Antonio, M., Florio, G., Paoletti, V., Morra, V., 2018. Gravity modeling finds a large magma body in the deep crust below the Gulf of Naples, Italy. Sci. Rep. 8, 8229. https://doi.org/10.1038/s41598-018-26346-z.
Forni, F., Bachmann, O., Mollo, S., De Astis, G., Gelman, S., Ellis, B.S., 2016. The origin of a zoned ignimbrite: Insights into the Campanian Ignimbrite magma chamber (Campi Flegrei, Italy). Earth Planet. Sci. Lett. 449, 259–271. https://doi.org/10.1016/J.EPSL.2016.06.003.
Forni, F., Degruyter, W., Bachmann, O., De Astis, G., Mollo, S., 2018. Long-term magmatic evolution reveals the beginning of a new caldera cycle at Campi Flegrei. Sci. Adv. 4, eaat9401. https://doi.org/10.1126/sciadv.aat9401.
Forte, F.M.L., Aiuppa, A., Rotolo, S.G., Zanon, V., 2023. Temporal evolution of the Fogo Volcano magma storage system (Cape Verde Archipelago): a fluid inclusions perspective. J. Volcanol. Geotherm. Res. 433, 107730. https://doi.org/10.1016/j.jvolgeores.2022.107730.
Fourmentraux, C., Métrich, N., Bertagnini, A., Rosi, M., 2012. Crystal fractionation, magma step ascent, and syn-eruptive mingling: the Averno 2 eruption (Phlegraean Fields, Italy). Contrib. Mineral. Petrol. 163, 1121–1137. https://doi.org/10.1007/s00410-012-0720-1.
Fowler, S.J., Spera, F.J., Bohrson, W.A., Belkin, H.E., De Vivo, B., 2007. Phase equilibria constraints on the chemical and physical evolution of the Campanian ignimbrite. J. Petrol. 48, 459–493. https://doi.org/10.1093/petrology/egl068.
Fulignati, P., Marianelli, M., Proto, M., Sbrana, A., 2004. Evidences for disruption of a crystallizing front in a magma chamber during caldera collapse: an example from the Breccia Museo unit (Campanian Ignimbrite eruption Italy). J. Volcanol. Geotherm. Res. 133, 141–155. https://doi.org/10.1016/S0377-0273(03)00395-0.
Fulignati, P., Boyce, A.J., 2023. Stable isotope ($\delta^{18}O$, δD) composition of magmatic fluids exsolved from an active alkaline magma chamber—The case of the AD 79 magma chamber of Vesuvius. Minerals 13, 913. https://doi.org/10.3390/min13070913.
Giaccio, B., Hajdas, I., Isaia, R., Deino, A., Nomade, S., 2017. High-precision ^{14}C and $^{40}Ar/^{39}Ar$ dating of the Campanian Ignimbrite (Y-5) reconciles the time-scales of climatic-cultural processes at 40 ka. Sci. Rep. 7, 45940. https://doi.org/10.1038/srep45940.
Giacomuzzi, G., Chiarabba, C., Bianco, F., De Gori, P., Piana Agostinetti, N., 2024. Tracking transient changes in the plumbing system at Campi Flegrei Caldera. Earth Planet. Sci. Lett. 637, 118744. https://doi.org/10.1016/j.epsl.2024.118744.
Herzberg, C.T., 1978. Pyroxene geothermometry and geobarometry: experimental and thermodynamic evaluation of some subsolidus phase relations involving pyroxenes in the system CaO-MgO-Al_2O_3-SiO_2. Geochim. Cosmochim. Acta 42, 945–957. https://doi.org/10.1016/0016-7037(78)90284-3.
Holloway, J.R., Blank, J.G., 1994. Chapter 6. Application of experimental results to C-O-H species in natural melts. In: Carroll, M.R., Holloway, J.R. (Eds.), Volatiles in Magmas, 30. De Gruyter, Berlin, Boston, pp. 187–230. https://doi.org/10.1515/9781501509674-012.
Isaia, R., D'Antonio, M., Dell'Erba, F., Di Vito, M., Orsi, G., 2004. The Astroni volcano: the only example of closely spaced eruptions in the same vent area during the recent history of the Campi Flegrei caldera (Italy). J. Volcanol. Geotherm. Res. 133, 171–192. https://doi.org/10.1016/S0377-0273(03)00397-4.
Kamenetsky, V., Métrich, N., Cioni, R., 1995. Potassic primary melts of Vulsini (Roman Province): evidence from mineralogy and melt inclusions. Contrib. Mineral. Petrol. 120, 186–196. https://doi.org/10.1007/BF00287116.
Kamenetsky, V.S., Kamenetsky, M.B., 2010. Magmatic fluids immiscible with silicate melts: examples from inclusions in phenocrysts and glasses, and implications for magma evolution and metal transport. Geofluids 10, 293–311. https://doi.org/10.1111/j.1468-8123.2009.00272.x.
Laporte, D., Lambart, S., Schiano, P., Ottolini, L., 2014. Experimental derivation of nepheline syenite and phonolite liquids by partial melting of upper mantle peridotites. Earth Planet. Sci. Lett. 404, 319–331. https://doi.org/10.1016/j.epsl.2014.08.002.
Lyubetskaya, T., Korenaga, J., 2007. Chemical composition of Earth's primitive mantle and its variance: 1. Method and results. J. Geophys. Res.: Sol. Earth 112, B03211. https://doi.org/10.1029/2005JB004223.
Lima, A., De Vivo, B., Spera, F.J., Bodnar, R.J., Milia, A., Nunziata, C., Belkin, H.E., Cannatelli, C., 2009. Thermodynamic model for uplift and deflation episodes (bradyseism) associated with magmatic–hydrothermal activity at the Campi Flegrei (Italy). Earth-Sci. Rev. 97, 44–58. https://doi.org/10.1016/j.earscirev.2009.10.001.
Lima, A., Bodnar, R.J., De Vivo, B., Spera, F.J., Belkin, H.E., 2021. Interpretation of recent unrest events (bradyseism) at Campi Flegrei, Napoli (Italy): comparison of models based on cyclical hydrothermal events versus shallow magmatic intrusive events. Geofluids 2021, 1–16. https://doi.org/10.1155/2021/2000255.
Lloyd, A.S., Plank, T., Ruprecht, F., Hauri, E.H., Rose, W., 2012. Volatile loss from melt inclusions in pyroclasts of differing sizes. Contrib. Mineral. 165, 129–153. https://doi.org/10.1007/s00410-012-0800-2.
Mangiacapra, A., Moretti, R., Rutherford, M., Civetta, L., Orsi, G., Papale, P., 2008. The deep magmatic system of the Campi Flegrei caldera (Italy). Geophys. Res. Lett. 35, L21304. https://doi.org/10.1029/2008GL035550.
Marianelli, P., Sbrana, A., Proto, M., 2006. Magma chamber of the Campi Flegrei supervolcano at the time of eruption of the Campanian ignimbrite. Geology 34, 937–940. https://doi.org/10.1130/G22807A.1.
Marini, L., Moretti, R., Accornero, M., 2011. Sulfur isotopes in magmatic-hydrothermal systems, melts, and magmas. Rev. Mineral. Geochem. 73, 423–492. https://doi.org/10.2138/rmg.2011.73.14.
Melluso, L., De' Gennaro, R., Fedele, L., Franciosi, L., Morra, V., 2012. Evidence of crystallization in residual, Cl-F-rich, agpaitic, trachyphonolitic magmas and primitive Mg-rich basalt-trachyphonolite interaction in the lava domes of the Phlegrean Fields (Italy). Geol. Mag. 149, 532–550. https://doi.org/10.1017/S0016756811000902
Monaco, L., Giaccio, B., Palladino, D.M., Albert, P.G., Arienzo, I., Conticelli, S., Di Vito, M., Fabbrizio, A., D'Antonio, M., Isaia, R., Manning, C.J., Nomade, S., Pereira, A., Petrosino, P., Sottili, G., Sulpizio, R., Zanchetta, G., 2022. Linking the Mediterranean MIS 5 tephra markers to Campi Flegrei (southern Italy) 109–92 ka explosive activity and refining the chronology of MIS 5c-d millennial-scale climate variability. Global Planet. Change 211, 103785. https://doi.org/10.1016/j.gloplacha.2022.103785.
Moore, G., 2008. Interpreting H_2O and CO_2 contents in melt inclusions: constraints from solubility experiments and modeling. Rev. Mineral. Geochem. 69, 333–362. https://doi.org/10.2138/rmg.2008.69.9.
Moretti, R., Papale, P., Ottonello, G., 2003. A model for the saturation of COHS fluids in silicate melts. Geol. Soc. Lond. Spec. Publ. 213, 81–101. https://doi.org/10.1144/GSL.SP.2003.213.01.06.
Moretti, R., Papale, P., 2004. On the oxidation state and volatile behaviour in multicomponent gas-melt equilibria. Chem. Geol. 213, 265–280. https://doi.org/10.1016/j.chemgeo.2004.08.048.
Moretti, R., Arienzo, I., Orsi, G., Civetta, L., D'Antonio, M., 2013a. The deep plumbing system of the Ischia Island: a physico-chemical window on the fluid-saturated and CO_2-sustained Neapolitan volcanism (Southern Italy). J. Petrol. 54, 951–984. https://doi.org/10.1093/petrology/egt002.
Moretti, R., Arienzo, I., Civetta, L., Orsi, G., Papale, P., 2013b. Multiple magma degassing sources at an explosive volcano. Earth Planet. Sci. Lett. 367, 95–104. https://doi.org/10.1016/j.epsl.2013.02.013.
Moretti, R., Métrich, N., Arienzo, I., Di Renzo, V., Aiuppa, A., Allard, P., 2018a. Degassing vs. eruptive styles at Mt. Etna volcano (Sicily, Italy). Part I: Volatile stocking, gas fluxing, and the shift from low-energy to highly explosive basaltic eruptions. Chem. Geol. 482, 1–17. https://doi.org/10.1016/j.chemgeo.2017.09.017.
Moretti, R., Troise, C., Sarno, F., De Natale, G., 2018b. Caldera unrest driven by CO_2-induced drying of the deep hydrothermal system. Sci. Rep. 8, 8309. https://doi.org/10.1038/s41598-018-26610-2.
Moretti, R., Arienzo, I., Di Renzo, V., Orsi, G., Arzilli, F., Brun, F., D'Antonio, M., Mancini, L., Deloule, E., 2019. Volatile segregation and generation of highly vesiculated explosive magmas by volatile-melt fining processes: the case of the Campanian ignimbrite eruption. Chem. Geol. 503, 1–14. https://doi.org/10.1016/j.chemgeo.2018.10.001.
Mormone, A., Piochi, M., Bellatreccia, F., De Astis, G., Moretti, R., Della Ventura, G., Cavallo, A., Mangiacapra, A., 2011. A CO_2–rich magma source beneath the Phlegraen volcanic district (southern Italy): evidence from a melt inclusion study. Chem. Geol. 287, 66–80. https://doi.org/10.1016/j.chemgeo.2011.05.019.
Orsi, G., de Vita, S., Di Vito, M.A., 1996. The restless resurgent Campi Flegrei nested caldera (Italy): constraints on its evolution and configuration. J. Volcanol. Geoth. Res. 74, 179–214. https://doi.org/10.1016/S0377-0273(96)00063-7.
Orsi, G., Di Vito, M.A., Isaia, R., 2004. Volcanic hazard assessment at the restless Campi Flegrei caldera. Bull. Volcanol. 66, 514–530. https://doi.org/10.1007/s00445-003-0336-4.
Orsi, G., Di Vito, M.A., Selva, J., Marzocchi, W., 2009. Long-term forecast of eruption style and size at Campi Flegrei caldera (Italy). Earth Planet. Sci. Lett. 287, 265–276. https://doi.org/10.1016/j.epsl.2009.08.013.
Orsi, G., 2022. Volcanic and deformation history of the Campi Flegrei volcanic field, Italy. In: Orsi, G., D'Antonio, M., Civetta, L. (Eds.), Campi Flegrei. Active Volcanoes of the World. Springer, Berlin, Heidelberg, pp. 1–53. https://doi.org/10.1007/978-3-642-37060-1_1.
Papale, P., Moretti, R., Barbato, D., 2006. The compositional dependence of the saturation surface of H_2O+CO_2 fluids in silicate melts. Chem. Geol. 229, 78–95. https://doi.org/10.1016/j.chemgeo.2006.01.013.
Papale, P., Moretti, R., Paonita, A., 2022. Thermodynamics of multi-component gas–melt equilibrium in magmas: Theory, models, and applications. Rev. Mineral. Geochem. 87, 431–556. https://doi.org/10.2138/rmg.2022.87.10.
Pappalardo, L., Ottolini, L., Mastrolorenzo, G., 2008. The Campanian Ignimbrite (southern Italy) geochemical zoning: insight on the generation of a super-eruption from catastrophic differentiation and fast withdrawal. Contrib. Mineral. Petrol. 156, 1–26. https://doi.org/10.1007/s00410-007-0270-0.
Pappalardo, L., Mastrolorenzo, G., 2012. Rapid differentiation in a sill-like magma reservoir: a case study from the Campi Flegrei caldera. Sci. Rep. 2, 712. https://doi.org/10.1038/srep00712.
Pappalardo, L., Buono, G., 2021. Insights into processes and timescales of magma storage and ascent from textural and geochemical investigations: case studies from high-risk Neapolitan volcanoes (Italy). In: Masotta, M., Beier, C., Mollo, S. (Eds.), Crustal Magmatic System Evolution: Anatomy, Architecture. and Physico-Chemical Processes. John Wiley & Sons Inc, pp. 213–235. https://doi.org/10.1002/9781119564485.ch10.
Pelullo, C., Iovine, R.S., Arienzo, I., Di Renzo, V., Pappalardo, L., Petrosino, P., D'Antonio, M., 2022a. Mineral-melt equilibria and geothermobarometry of

Campi Flegrei magmas: Inferences for magma storage conditions. Minerals 12, 308. https://doi.org/10.3390/min12030308.
Pelullo, C., Chakraborty, S., Cambeses, A., Dohmen, R., Arienzo, I., D'Antonio, M., Pappalardo, L., Petrosino, P., 2022b. Insights into the temporal evolution of magma plumbing systems from compositional zoning in clinopyroxene crystals from the Agnano-Monte Spina Plinian eruption (Campi Flegrei, Italy). Geochim. Cosmochim. Acta 328, 185–206. https://doi.org/10.1016/j.gca.2022.04.007.
Perinelli, C., Gaeta, M., Bonechi, B., Granati, S.F., Freda, C., D'Antonio, M., Stagno, V., Sicola, S., Romano, C., 2019. Effect of water on the phase relations of primitive K-basalts: Implications for high-pressure differentiation in the Phlegraean volcanic district magmatic system. Lithos 342–343, 530–541. https://doi.org/10.1016/j.lithos.2019.05.032.
Perrotta, A., Scarpati, C., Luongo, G., Morra, V., 2006. The Campi Flegrei caldera boundary in the city of Naples. In: De Vivo, B. (Ed.). Volcanism in the Campania Plain: Vesuvius, Campi Flegrei and Ignimbrites. Developments in Volcanology, Elsevier 9, 85–96. https://doi.org/10.1016/s1871-644x(06)80019-7.
Pino, N.A., Moretti, R., Allard, P., Boschi, E., 2011. Seismic precursors of a basaltic paroxysmal explosion track deep gas accumulation and slug upraise. J. Geophys. Res. 116, B02312. https://doi.org/10.1029/2009JB000826.
Pistolesi, M., Isaia, R., Marianelli, P., Bertagnini, A., Fourmentraux, C., Albert, P.G., Tomlinson, E.L., Menzies, M.A., Rosi, M., Sbrana, A., 2016. Simultaneous eruptions from multiple vents at Campi Flegrei (Italy) highlight new eruption processes at calderas. Geology 44, 487–490. https://doi.org/10.1130/G37870.1.
Putirka, K., 2008. Thermometers and barometers for volcanic systems. Rev. Mineral. Geochem. 69, 61–120. https://doi.org/10.2138/rmg.2008.69.3.
Roach, A.L., 2005. The evolution of silicic magmatism in the post-caldera volcanism of the Phlegrean Fields, Italy. Ph.D. thesis, Brown University, Providence, USA, p.151.
Santacroce, R., Cristofolini, R., La Volpe, L., Orsi, G., Rosi, M., 2003. Italian active volcanoes. Episodes 26, 227–234. https://doi.org/10.18814/epiiugs/2003/v26i3/013.
Sbrana, A., Marianelli, P., Pasquini, G., 2021. The Phlegrean Fields volcanological evolution. J. Maps 17 (2), 557–570. https://doi.org/10.1080/17445647.2021.1982033.
Selva, J., Orsi, G., Di Vito, M.A., Marzocchi, W., Sandri, L., 2012. Probability hazard map for future vent opening at the Campi Flegrei caldera, Italy. Bull. Volcanol. 74, 497–510. https://doi.org/10.1007/s00445-011-0528-2.
Severs, M.J., 2007. Applications of melt inclusions to problems in igneous petrogenesis. M.S. thesis, Virginia Tech, Blacksburg, VA, USA. p. 118.
Seyler, M., Bonatti, E., 1994. Na, Al^{IV} and Al^{VI} in clinopyroxenes of subcontinental and suboceanic ridge peridotites: a clue to different melting processes in the mantle? Earth Planet Sci. Lett. 122, 281–289. https://doi.org/10.1016/0012-821X(94)90002-7.
Signorelli, S., Vaggelli, G., Francalanci, L., Rosi, M., 1999. Origin of magmas feeding the Plinian phase of the Campanian ignimbrite eruption (Phlegrean Fields Italy): constraints based on matrix glass and glass inclusion compositions. J. Volcanol. Geotherm. Res. 91, 199–220. https://doi.org/10.1016/S0377-0273(99)00036-0.
Signorelli, S., Vaggelli, G., Romano, C., Carroll, M.R., 2001. Volatile element zonation in Campanian Ignimbrite magmas (Phlegrean Fields Italy): evidence from the study of glass inclusion and matrix glasses. Contrib. Mineral. Petrol. 140, 543–553. https://doi.org/10.1007/s004100000213.
Smith, V.C., Isaia, R., Pearce, N.J.G., 2011. Tephrostratigraphy and glass compositions of post-15 kyr Campi Flegrei eruptions: implications for eruption history and chronostratigraphic markers. Quat. Sci. Rev. 30, 3638–3660. https://doi.org/10.1016/j.quascirev.2011.07.012.
Sparice, D., Pelullo, C., de Vita, S., Arienzo, I., Petrosino, P., Mormone, A., Di Vincenzo, G., Marfè, B., Cariddi, B., De Lucia, M., Vertechi, E., D'Oriano, C., Del Carlo, P., Di Roberto, Giaccio, B., Zanchetta, G., Di Vito, M.A., 2024. The pre-Campi Flegrei caldera (> 40 ka) explosive volcanic record in the Neapolitan Volcanic Area: New insights from a scientific drilling north of Naples, southern Italy. J. Volcanol. Geotherm. Res. 455, 108209. https://doi.org/10.1016/j.jvolgeores.2024.108209.
Spilliaert, N., Allard, P., Metrich, N., Sobolev, A.V., 2006. Melt inclusion record of the conditions of ascent, degassing, and extrusion of volatile-rich alkali basalt during the powerful 2002 flank eruption of Mount Etna (Italy). J. Geophys. Res. 111, 19. https://doi.org/10.1029/2005JB003934.
Steele-Macinnis, M., Esposito, R., Bodnar, R.J., 2011. Thermodynamic model for the effect of post-entrapment crystallization on the H_2O–CO_2 systematics of vapor-saturated, silicate melt inclusions. J. Petrol. 52, 2461–2482. https://doi.org/10.1093/petrology/egr052.
Suzuoki, T., Epstein, S., 1976. Hydrogen isotope fractionation between OH-bearing minerals and water. Geochim. Cosmochim. Acta 40 (10), 1229–1240. https://doi.org/10.1016/0016-7037(76)90158-7.
Taylor, B.E., 1986. Magmatic volatiles: isotopic variation of C, H, and S. In: Valley, J. W., Taylor, H.P., O'Neil, J.R. (Eds.), Stable Isotopes in High Temperature Geological Processes. Reviews in Mineralogy, Mineralogical Society of America, Washington, D.C., vol. 16., pp. 185–225. https://doi.org/10.1515/9781501508936-008.
Thompson, R.N., 1974. Some high-pressure pyroxenes. Mineral. Mag. 39, 768–787. https://doi.org/10.1180/minmag.1974.039.307.04.
Tonarini, S., D'Antonio, M., Di Vito, M.A., Orsi, G., Carandente, A., 2009. Geochemical and B-Sr-Nd evidence for mingling and mixing processes in the magmatic system feeding the Astroni volcano (4.1–3.8 ka) within the Campi Flegrei caldera (South Italy). Lithos 107, 135–151. https://doi.org/10.1016/j.lithos.2008.09.012.
Tramelli, A., Giudicepietro, F., Ricciolino, P., Chiodini, G., 2022. The seismicity of Campi Flegrei in the contest of an evolving long term unrest. Sci. Rep. 12, 2900. https://doi.org/10.1038/s41598-022-06928-8.
Vetere, F., Botcharnikov, R.E., Holtz, F., Behrens, H., De Rosa, R., 2011. Solubility of H_2O and CO_2 in shoshonitic melts at 1250 °C and pressures from 50 to 400 MPa: implications for Campi Flegrei magmatic systems. J. Volcanol. Geotherm. Res. 202, 251–261. https://doi.org/10.1016/j.jvolgeores.2011.03.002.
Villemant, B., 1988. Trace-element evolution in the Phlegrean Fields (central-Italy)-fractional crystallization and selective enrichment. Contr. Mineral. Petrol. 98, 169–183.
Vitale, S., Isaia, R., 2014. Fractures and faults in volcanic rocks (Campi Flegrei, southern Italy): Insight into volcano-tectonic processes. Int. J. Earth Sci. 103 (3), 801–819. https://doi.org/10.1007/s00531-013-0979-0.
Voloschina, M., Pistolesi, M., Bertagnini, A., Métrich, N., Pompilio, M., Di Roberto, A., Di Salvo, S., Francalanci, L., Isaia, R., Cioni, R., Romano, C., 2018. Magmatic reactivation of the Campi Flegrei volcanic system: insights from the Baia–Fondi di Baia eruption. Bull. Volcanol. 80, 75. https://doi.org/10.1007/s00445-018-1247-8.
Webster, J.D., Raia, F., Tappen, C., De Vivo, B., 2003. Pre-eruptive geochemistry of the ignimbrite-forming magmas of the Campanian Volcanic Zone, Southern Italy, determined from silicate melt inclusions. Mineral. Petrol. 79, 99–125. https://doi.org/10.1007/s00710-003-0004-6.
Zanon, V., D'Auria, L., Schiavi, F., Cyrzan, K., Pankhurst, M.J., 2024. Toward a near real-time magma ascent monitoring by combined fluid inclusion barometry and ongoing seismicity. Sci. Adv. 10, eadi4300. https://doi.org/10.1126/sciadv.adi4300.
Zollo, A., Maercklin, N., Vassallo, M., Dello Iacono, D., Virieux, J., Gasparini, P., 2008. Seismic reflections reveal a massive melt layer feeding Campi Flegrei caldera. Geophys. Res. Lett. 35, L12306. https://doi.org/10.1029/2008GL034242.